TRANSPORT PHENOMENA FOR CHEMICAL REACTOR DESIGN

1. Introduction

The topics discussed in this article allow one to include principles from coupled heat and mass transfer in the design of plug-flow tubular reactors that are packed with porous catalysts. When one chemical reaction occurs on the internal catalytic surface, stoichiometric relations are discussed that relate temperature and reactant molar density on the external catalytic surface to their counterparts in the bulk fluid phase. These relations are combined with coupled species mass and thermal energy balances in differential plug-flow tubular reactors to predict temperature and conversion profiles as a function of reactor length. Important dimensionless parameters are defined and quantified to determine the significance of external mass transfer resistance and interpellet axial dispersion in nonideal reactors. The combination of external mass transfer resistance and interpellet axial dispersion in nonideal packed catalytic tubular reactors is simulated numerically to identify conditions that yield maximum conversion of reactants to products. These simulations emphasize the importance of nonideal

analysis because maximum conversion invariably occurs at subcritical values of the mass transfer Peclet number where interpellet axial dispersion must be included in the design equations. Furthermore, rates of reactant conversion must be evaluated at molar densities near the external catalytic surface, which are different from those in the bulk fluid phase, because external mass transfer resistance in packed catalytic tubular reactors cannot be neglected in most designs that seek maximum conversion. Important design parameters, such as volumetric flowrate, particle size, and reactor diameter (but not length), and their effects on external mass transfer resistance are discussed via illustrative examples that include numerical calculations and universal scaling laws. Intrapellet resistances are considered from the viewpoint of maximum temperature in adiabatic pellets when exothermic chemical reactions occur. This analysis of coupled heat and mass transfer in isolated porous catalysts includes contributions from Fourier's law and the interdiffusional flux to quantify the molecular flux of thermal energy, as well as a combination of Fick's law and thermal diffusion to describe diffusional mass flux in macropores where collisions among molecules govern the resistance to intrapellet mass transfer. Numerical predictions of adiabatic temperature increases for exothermic reaction within porous catalysts exceed previous estimates of this temperature rise via the classic Prater equation when the dimensionless Prater number approaches unity and all physicochemical properties of the catalyst exhibit temperature dependence. All of these concepts are considered to develop a complete design strategy for the synthesis of methanol from a stoichiometric feed of carbon monoxide and hydrogen in nonisothermal packed catalytic tubular reactors. Realistic simulations that employ thermodynamic data for all three components in this industrially important exothermic reaction at moderately high pressure yield temperature and conversion profiles, which indicate that 35% conversion of carbon monoxide to methanol should be achieved. Finally, suggestions are proposed to limit the approximate 80°C temperature increase that occurs near the reactor inlet when the rate of thermal energy generation due to exothermic chemical reaction exceeds the rate of heat removal across the lateral diathermal wall of the tube. Numerical integration of ordinary differential equations is employed extensively throughout this article. Results are presented in graphical and tabular form to illustrate the trends that develop. In most cases, these trends and their associated strategies are not unique to a specific chemical reaction, so the universal nature of the topics discussed in this article deserves merit.

2. Methodology

The dilemma can be summarized as follows. Plug-flow mass and thermal energy balances in packed catalytic tubular reactors are written in terms of molar densities and temperature in the bulk fluid (ie, gas) phase. However, the volumetrically averaged rate of reactant consumption within catalytic pellets is calculated, with assistance from effectiveness factor correlations, via molar densities and temperature on the external surface of the pellets. When external transport resistances are negligible, the design of these reactors is simplified by equating bulk gas-phase conditions to those on the external catalytic surface.

This article addresses the dilemma when external heat and mass transfer resistances cannot be neglected because bulk gas-phase conditions are different from those on the external surface of the pellet. The logical sequence of calculations is as follows:

(1) Invoke stoichiometry and the mass balance with diffusion and only one chemical reaction within isolated catalytic pellets to relate intrapellet diffusional mass fluxes among all reactants and products.
(2) Invoke continuity of the normal component of diffusional mass fluxes on both sides of the gas/porous–solid interface. Then, use interphase mass transfer coefficients within the gas-phase boundary layer surrounding the pellets to evaluate interfacial molar fluxes and relate molar densities in the bulk fluid phase and on the external surface of the catalyst.
(3) Simplify the multicomponent thermal energy balance in the gas-phase boundary layer that surrounds each catalytic pellet. Then, (a) evaluate all fluxes at the gas/porous–solid interface, (b) invoke continuity of the normal component of diffusional mass flux for each component on both sides of the interface, and (c) introduce mass and heat transfer coefficients to calculate these interfacial fluxes.

External resistances to heat and mass transfer can be expressed in terms of the difference between molar densities of key reactant A in the bulk gas phase and on the external surface of the catalyst; $C_{A,\mathrm{BulkGas}} - C_{A,\mathrm{Surface}}$. Integration of the plug-flow mass balance, together with the thermal energy balance for nonisothermal systems, allows one to calculate temperature T_{Bulk} and the concentration of reactant A, $C_{A,\mathrm{BulkGas}}$, in the bulk gas phase. The critical step involves determination of $C_{A,\mathrm{Surface}}$ in terms of $C_{A,\mathrm{BulkGas}}$ via effectiveness factor formalism. In other words, the rate of interphase mass transfer of key reactant A from the bulk gas phase to the external surface of the catalyst is balanced by a volumetric average of the rate of consumption of reactant A within the pellet at steady state.

2.1. Stoichiometry and the Steady-State Mass Balance with Diffusion and Chemical Reaction in Porous Catalytic Pellets. Contributions from convective transport are negligible in porous catalysts. Hence, one begins with the steady-state microscopic mass transfer equation that includes pseudohomogeneous diffusion and multiple pseudo-volumetric chemical reactions for component i:

$$\frac{\partial C_i}{\partial t} + v \cdot \nabla C_i \underbrace{\overbrace{\Longrightarrow}^{\text{steady state}}}_{\text{negligible convective transport}} 0 = -\nabla \cdot \left\{ \frac{j_{i,\mathrm{pellet}}}{MW_i} \right\} + \underbrace{\sum_k v_{ik} R_k}_{\text{reactions}} \tag{1}$$

where C_i is the molar density of component i with molecular weight MW_i, $\mathbf{j}_{i,\mathrm{pellet}}$ represents the intrapellet diffusional mass flux of species i with respect to a reference frame that translates at the mass-average velocity $\mathbf{v} \approx 0$ of the reactive

mixture, υ_{ik} is the stoichiometric coefficient of species i in reaction k, and R_k is the intrinsic rate of the kth chemical reaction. Stoichiometric relations are exceedingly complex in the presence of multiple chemical reactions (1). In light of this complexity, the current problem is addressed for only one chemical reaction on the internal catalytic surface. Now, subscript k is not required, and the previous mass balance with intrapellet diffusion and one chemical reaction yields the following stoichiometric relation that is the *same for each component in the reactive mixture*:

$$\frac{1}{\upsilon_i MW_i}\nabla \cdot j_{i,\text{pellet}} = \frac{1}{\upsilon_A MW_A}\nabla \cdot j_{A,\text{pellet}} = R \tag{2}$$

Stoichiometric relations are generated from the mass balance by isolating all quantities that are *species specific* (ie, containing subscript i). Equation 2 is integrated over an arbitrary control volume V within the catalytic pores via Gauss' law, yielding equation 3:

$$\begin{aligned}&\int_V \left\{\frac{1}{\upsilon_i MW_i}\nabla \cdot j_{i,\text{pellet}} - \frac{1}{\upsilon_A MW_A}\nabla \cdot j_{A,\text{pellet}}\right\} dV \\ &= \int_S \left\{\frac{1}{\upsilon_i MW_i}\underline{n} \cdot j_{i,\text{pellet}} - \frac{1}{\upsilon_A MW_A}\underline{n} \cdot j_{A,\text{pellet}}\right\}_{@S} dS = 0\end{aligned} \tag{3}$$

where $\underline{\mathbf{n}}$ is a unit normal vector directed *outward* from the surface of the control volume. As there are many choices for control volume V and surface S that surrounds this volume element, the integrand of the surface integral must vanish. Hence:

$$\frac{1}{\upsilon_i MW_i}\{\underline{n} \cdot j_{i,\text{pellet}}\}_{@S} = \frac{1}{\upsilon_A MW_A}\{\underline{n} \cdot j_{A,\text{pellet}}\}_{@S} \tag{4}$$

It should be emphasized that this stoichiometric relation generated from the microscopic mass transfer equation with diffusion and one chemical reaction is valid at any surface S that surrounds control volume V within the pellet.

2.2. Species Concentrations in the Bulk Gas Phase. When the stoichiometric relation for intrapellet diffusional mass fluxes in the catalytic pores is evaluated at the external surface of the catalyst, it is possible to (*1*) invoke continuity across the gas/porous–solid interface, and (*2*) introduce mass transfer coefficients to evaluate interfacial fluxes. Now, $\underline{\mathbf{n}}$ represents the *outward* directed unit normal vector from the external surface of the catalyst into the bulk gas phase. A steady-state balance for any reactive species at the gas/porous–solid interface allows one to invoke continuity of the normal component of mass flux (ie, $\underline{\mathbf{n}}\cdot\rho_i\mathbf{v}_i$) on both sides of the interface, even though chemical reaction occurs on the pellet-side of the interface but not in the bulk gas phase. Hence, on the external surface of the catalyst, one writes:

$$\{\underline{n} \cdot j_{i,\text{pellet}}\}_{\text{External Surface}} = \{\underline{n} \cdot j_{i,\text{BulkGas}}\}_{\text{External Surface}} \tag{5}$$

because convective mass transfer is negligible in both phases at the interface. Bulk gas-phase molar densities are introduced into the stoichiometric relation by evaluating the normal component of these interfacial *molar* fluxes in terms of a mass transfer coefficient $k_{i,\mathrm{MTC}}$ and a concentration driving force, which is standard procedure for interphase transport. Hence:

$$\frac{1}{MW_i}\{\underline{n}\cdot j_{i,\mathrm{BulkGas}}\}_{\mathrm{External\ Surface}} = k_{i,\mathrm{MTC}}(C_{i,\mathrm{Surface}} - C_{i,\mathrm{BulkGas}}) \tag{6}$$

Now, the intrapellet stoichiometric relations among diffusional mass fluxes at the gas/porous−solid interface (ie, eqs. 4–6) are expressed in terms of surface and bulk gas-phase concentrations:

$$\frac{1}{\upsilon_i}k_{i,\mathrm{MTC}}(C_{i,\mathrm{Surface}} - C_{i,\mathrm{BulkGas}}) = \frac{1}{\upsilon_A}k_{A,\mathrm{MTC}}(C_{A,\mathrm{Surface}} - C_{A,\mathrm{BulkGas}}) \tag{7}$$

Since the stoichiometric coefficient of reactant A, $\upsilon_A = -1$, it is possible to relate molar densities on the external surface of the catalyst to those in the bulk gas phase:

$$C_{i,\mathrm{Surface}} - C_{i,\mathrm{BulkGas}} = \upsilon_i \frac{k_{A,\mathrm{MTC}}}{k_{i,\mathrm{MTC}}}(C_{A,\mathrm{BulkGas}} - C_{A,\mathrm{Surface}}) \tag{8}$$

This equation correctly predicts that $C_{i,\mathrm{Surface}} - C_{i,\mathrm{BulkGas}}$ is positive for products and negative for reactants, because $C_{A,\mathrm{BulkGas}} > C_{A,\mathrm{Surface}}$ for key reactant A. The kinetic rate law is evaluated on the external surface of the pellet, and the defining equation for the effectiveness factor is employed to predict the average rate of reactant consumption on the internal surface of the catalyst. When molar densities on the external surface are required in the kinetic rate law, the previous equation should be employed to re-express $C_{i,\mathrm{Surface}}$ in terms of bulk gas phase conditions. This is advantageous because the plug-flow mass balance for species i is written in terms of $C_{i,\mathrm{BulkGas}}$.

2.3. Temperature on the External Catalytic Surface and in the Bulk Gas Phase. The primary objective of this section is to evaluate temperature on the external surface of the catalyst in terms of bulk gas-phase temperature and the molar density of key reactant A at the external catalytic surface and in the bulk gas phase. This is accomplished from steady-state analysis of coupled heat and mass transfer in the thermal boundary layer external to an isolated pellet, where no chemical reaction occurs. The thermal energy balance is written in terms of specific internal energy u for an N-component mixture, prior to invoking any assumptions:

$$\frac{\partial \rho u}{\partial t} + \nabla\cdot\rho v u = -\nabla\cdot\underline{q} - p\nabla\cdot v - \tau : \nabla v + \sum_{i=1}^{N} j_{i,\mathrm{BulkGas}}\cdot g_i \tag{9}$$

The molecular flux of thermal energy in this N-component mixture is (2)

$$\underline{q} = -k_{\mathrm{TC}}\nabla T + \sum_{i=1}^{N}\frac{\bar{H}_i}{MW_i}j_{i,\mathrm{BulkGas}} \tag{10}$$

Fourier's law with thermal conductivity k_{TC} of the gas phase medium surrounding each pellet describes the first term on the right side of the previous equation, and the inter-diffusional flux that contains products of partial molar enthalpy and diffusional mass flux of each component in the summation accounts for the most important coupling between heat and mass transfer. The diffusion-thermo (ie, Dufour) effect is neglected in the previous expression for the molecular flux of thermal energy. The following rate processes are neglected in the microscopic thermal energy balance (2):

(1) Reversible exchange between internal and kinetic energies (ie, $p\ \nabla\cdot\mathbf{v} \Rightarrow 0$)
(2) Irreversible conversion of kinetic energy to internal energy (ie, $\tau:\nabla\mathbf{v} \Rightarrow 0$)
(3) External force field effects (ie, $\sum_{1\le i\le N} \mathbf{j}_{i,\mathrm{BulkGas}}\cdot\ \mathbf{g}_i \Rightarrow 0$)

Hence, the complex thermal energy balance given by equation 9 is simplified considerably for steady-state analysis in the external gas-phase boundary layer

$$\nabla\cdot\{\rho v u + \underline{q}\} = 0 \tag{11}$$

when contributions from convective transport are not neglected. Integration of the previous equation over an arbitrary control volume V within the external heat transfer boundary layer via Gauss' law yields

$$\int_V [\nabla\cdot\{\rho v u + \underline{q}\}]dV = \int_S [\underline{n}\cdot\{\rho v u + \underline{q}\}]_{@S} dS = 0 \tag{12}$$

where $\underline{\mathbf{n}}$ is a unit normal vector directed outward from surface S that surrounds control volume V. As there are many choices for control volume V and surface S that surrounds this volume element in the thermal boundary layer, the integrand of the surface integral vanishes. Hence,

$$[\underline{n}\cdot\{\rho v u + \underline{q}\}]_{@S} = \underline{n}\cdot\left\{\rho v u - k_{\mathrm{TC}}\nabla T + \sum_{i=1}^{N}\frac{\bar{H}_i}{MW_i} j_{i,\mathrm{BulkGas}}\right\}_{@S} = 0 \tag{13}$$

The previous equation is evaluated on the external surface of the catalyst, where $\underline{\mathbf{n}}$ represents the unit normal vector directed into the pellet and convective transport is negligible. In other words, the bulk gas phase velocity in the normal coordinate direction (ie, $\underline{\mathbf{n}}\cdot\mathbf{v}$) is neglected on the external surface of the catalyst where molecular fluxes provide the dominant contributions to heat and mass transfer. The mass flux of component i normal to the external gas/porous−solid interface must be continuous. Hence, $\underline{\mathbf{n}}\cdot\mathbf{j}_i$ is the same on each side of the interface when convective transport is unimportant (see eq. 5). When the previous equation is evaluated on the external surface of the pellet and $\underline{\mathbf{n}}\cdot\mathbf{j}_{i,\mathrm{BulkGas}}$ in the external boundary layer is replaced by its counterpart in the porous catalyst, one invokes the stoichiometric relation among intrapellet

diffusional mass fluxes that was derived earlier in this article (see eq. 4). The result is

$$\begin{aligned}[\underline{n}\cdot\{k_{\mathrm{TC}}\nabla T\}]_{\text{External Surface}} &= \sum_{i=1}^{N}\frac{\bar{H}_i}{MW_i}\{\underline{n}\cdot j_{i,\text{BulkGas}}\}_{\text{External Surface}}\\ &= \sum_{i=1}^{N}\upsilon_i\bar{H}_i\,\frac{1}{\upsilon_i MW_i}\{\underline{n}\cdot j_{i,\text{pellet}}\}_{\text{External Surface}}\\ &= \frac{1}{\upsilon_A MW_A}\{\underline{n}\cdot j_{A,\text{pellet}}\}_{\text{External Surface}}\sum_{i=1}^{N}\upsilon_i\bar{H}_i\\ &\underset{\upsilon_A=-1}{\Rightarrow}\frac{1}{MW_A}\{\underline{n}\cdot j_{A,\text{pellet}}\}_{\text{External Surface}}(-\Delta H_{\text{Reaction}}) \qquad (14)\end{aligned}$$

where the stoichiometric coefficient of reactant A is -1. The summation over all species in the reactive mixture of products of stoichiometric coefficient and partial molar enthalpy is an exact representation of the enthalpy change for chemical reaction, $\Delta H_{\text{Reaction}}$, on a molar basis (3). Intermolecular interactions and nonideal heats of solution are also included in

$$\sum_{i=1}^{N}\upsilon_i\bar{H}_i = \Delta H_{\text{Reaction}} \approx \Delta H^0_{\text{Rx,298K}} + \sum_{i=1}^{N}\upsilon_i\int_{298\text{K}}^{T} C_{p,i}(T)dT \qquad (15)$$

because the summation on the left side of equation 15 contains partial molar enthalpies. In practice, one estimates $\Delta H_{\text{Reaction}}$ using literature values for standard state enthalpies of formation at 298K and temperature "polynomials" for pure-component specific heats. This approximation is exact for ideal solutions because partial molar enthalpies reduce to pure-component molar enthalpies under ideal conditions. Temperatures in the bulk gas phase and on the external surface of the catalyst are related to the corresponding molar densities of key reactant A by focusing on the external heat and mass transfer boundary layers surrounding each catalytic pellet. The normal components of conductive and diffusional fluxes on the bulk gas-phase side of the gas/porous–solid interface are written in terms of a transfer coefficient and a driving force, the latter of which is sensitive to the direction of the unit normal vector $\underline{\mathbf{n}}$ and the fact that Fourier's law and Fick's law require a negative sign to calculate fluxes in a particular coordinate direction. These considerations produce the following expressions for the conductive energy flux:

$$[-\underline{n}\cdot\{-k_{\mathrm{TC}}\nabla T\}]_{\text{External Surface}} = h_{\mathrm{HTC}}(T_{\text{Surface}} - T_{\text{BulkGas}}) \qquad (16)$$

and the diffusional molar flux of reactant A with respect to the mass-average reference frame:

$$\begin{aligned}\frac{1}{MW_A}\{\underline{n}\cdot j_{A,\text{pellet}}\}_{\text{External Surface}} &= \frac{1}{MW_A}\{\underline{n}\cdot j_{A,\text{BulkGas}}\}_{\text{External Surface}}\\ &= k_{A,\mathrm{MTC}}(C_{A,\text{BulkGas}} - C_{A,\text{Surface}}) \qquad (17)\end{aligned}$$

In both cases, these fluxes are normal to the gas/porous–solid interface, and $\underline{\mathbf{n}}$ is the unit normal vector directed into the catalyst. The temperature difference between the external surface of the catalytic pellet and the bulk gas stream is estimated via equations 14–17;

$$T_{\text{Surface}} - T_{\text{BulkGas}} = (-\Delta H_{\text{Reaction}}) \frac{k_{A,\text{MTC}}}{h_{\text{HTC}}} \{C_{A,\text{BulkGas}} - C_{A,\text{Surface}}\} \qquad (18)$$

which reveals that $T_{\text{Surface}} > T_{\text{BulkGas}}$ for exothermic chemical reactions (ie, negative $\Delta H_{\text{Reaction}}$), because $C_{A,\text{BulkGas}} > C_{A,\text{Surface}}$ for reactant A. Heat and mass transfer coefficients in the external boundary layers (ie, h_{HTC} and $k_{A,\text{MTC}}$) are enhanced by convective transport parallel to the gas/porous–solid interface, and hence, they are functions of the Reynolds and Prandtl or Schmidt numbers, as discussed later in this article.

2.4. Evaluation of $C_{A,\text{Surface}}$ via the Effectiveness Factor. The microscopic mass balance with pseudo-homogeneous one-dimensional diffusion and pseudo-volumetric irreversible nth-order chemical reaction provides basic information for the spatial dependence of reactant molar density within an isolated catalytic pellet. Analytical or numerical solutions for the molar density profile can be obtained for any type of chemical kinetics (2). Analytical solutions are only available when the rate law conforms to simple zeroth-order or first-order kinetics. Numerical solutions of two-coupled first-order ordinary differential equations with split boundary conditions are required when the kinetics are more complex. The rationale for developing correlations between the effectiveness factor and the intrapellet Damköhler number (ie, dimensionless ratio of the rate of chemical reaction to the rate of intrapellet diffusion) is based on the fact that the reactor design engineer does not want to consider the details of the interplay between diffusion and chemical reaction in each catalytic pellet when these pellets are packed in a large-scale reactor. The effectiveness factor strategy is formulated as follows:

(1) Account for pseudo-homogeneous diffusion and pseudo-volumetric chemical reaction in one isolated catalytic pellet, and calculate a volumetrically averaged rate of consumption of reactants within the pellet in terms of conditions on the external surface of the catalyst.
(2) The volume-averaged rate of reaction in each catalytic pellet is incorporated into plug-flow mass and thermal energy balances to predict reactor performance.

Condition (1) is addressed by using basic information from the mass balance to evaluate the effectiveness factor. The ratio of reaction rates described in (a) and (b) below, with units of moles per time, is defined as the effectiveness factor:

(a) The volume-averaged rate of consumption of reactants in one isolated catalytic pellet, relative to

(b) the rate of consumption of reactant A evaluated using conditions on the external surface of the pellet

A generalized expression for the volume-averaged rate of consumption of reactant A, specified by (a), is

$$-\upsilon_A \int_{V_{\text{catalyst}}} R(C_{A,\text{pellet}})dV$$

where integration is performed over the entire volume of the catalyst if reactant A exists everywhere throughout the catalyst. A modification of the integration limits is required for zeroth-order kinetics when the intrapellet Damköhler number is larger than its critical value and the central core of the catalyst is void of reactants. The rate of consumption of reactant A based on external surface conditions, specified by (b), is

$$-\upsilon_A R(C_{A,\text{Surface}})V_{\text{catalyst}}$$

where V_{catalyst} represents the entire volume of one pellet because the molar density of reactant A is assumed to be $C_{A,\text{Surface}}$ everywhere throughout the catalyst. In both of the previous expressions, the pseudo-volumetric reaction rate R, with dimensions of moles per pellet volume per time, is related to the heterogeneous catalytic rate law R_{Surface} (ie, moles per internal catalytic surface area per time) via internal structural characterstics of each porous pellet, $R = S_m \rho_{\text{apparent}} R_{\text{Surface}}$, where S_m is the internal catalytic surface area per pellet mass and ρ_{apparent} is the apparent density of each porous pellet, including the intrapellet void volume. The general expression for the effectiveness factor is

$$E = \frac{\int_{V_{\text{catalyst}}} R(C_{A,\text{pellet}})dV}{R(C_{A,\text{Surface}})V_{\text{catalyst}}} \tag{19}$$

when the kinetics are averaged throughout the volume of one pellet. An equivalent expression for the volume-averaged rate of consumption of reactant A (ie, the numerator of the effectiveness factor in equation 19) is based on mass flux of reactant A into the pellet across the external surface. Under steady-state conditions, the microscopic mass transfer equation for component A with pseudo-homogeneous diffusion and one pseudo-volumetric chemical reaction is (see equation 2);

$$\frac{1}{MW_A} \nabla \cdot j_{A,\text{pellet}} = \upsilon_A R \tag{2}$$

Integration over the entire volume of one catalytic pellet allows one to calculate the volume-averaged rate at which reactant A is consumed by chemical reaction on the interior catalytic surface:

$$-\upsilon_A \int_{V_{\text{catalyst}}} R(C_{A,\text{pellet}})dV = -\frac{1}{MW_A}\int_{V_{\text{catalyst}}} \{\nabla \cdot j_{A,\text{pellet}}\}dV$$

$$= -\frac{1}{MW_A}\int_{S_{\text{external}}} \{\underline{n} \cdot j_{A,\text{pellet}}\}_{@S_{\text{external}}}dS = -\frac{1}{MW_A}\int_{S_{\text{external}}} \{\underline{n} \cdot j_{A,\text{BulkGas}}\}_{@S_{\text{external}}}dS \tag{20}$$

Gauss' law was employed to transform the volume integral of $\nabla \cdot \mathbf{j}_{A,\text{pellet}}$ to an integral over the external catalytic surface of $\underline{\mathbf{n}} \cdot \mathbf{j}_{A,\text{pellet}}$, continuity of the normal component of diffusional mass flux at the gas/porous−solid interface was adopted from equation 5, and $\underline{\mathbf{n}}$ is an *outward* directed unit normal vector from the external surface of the catalyst to the bulk gas phase. Hence, the volume-averaged rate of consumption of reactant A via chemical reaction is equivalent to the surface-averaged rate of diffusion of A *into* the catalyst (ie, in the direction of $-\underline{\mathbf{n}}$). For one-dimensional problems that are characteristic of pseudo-homogeneous diffusion and pseudo-volumetric chemical reaction in catalytic pellets, the molar density of reactant A, its gradient, and its diffusional mass flux are not functions of the surface coordinates that comprise the differential surface element dS on the external surface of a single pellet. Hence, the numerator of the effectiveness factor can be simplified and rewritten in terms of a gas-phase mass transfer coefficient and the difference between reactant A's molar density in the bulk gas phase and on the external surface of the catalyst via equation 6.

$$-\upsilon_A \int_{V_{\text{catalyst}}} R(C_{A,\text{pellet}})dV = -\frac{1}{MW_A}\int_{S_{\text{external}}} \{\underline{n} \cdot j_{A,\text{BulkGas}}\}_{@S_{\text{external}}}dS$$

$$= -\frac{1}{MW_A}\{\underline{n} \cdot j_{A,\text{BulkGas}}\}_{@S_{\text{external}}}S_{\text{external}} = k_{A,\text{MTC}}(C_{A,\text{BulkGas}} - C_{A,\text{Surface}})S_{\text{external}} \tag{21}$$

Effectiveness factor formalism (ie, eq. 19) has been employed to evaluate the molar density of key reactant A on the external catalytic surface, $C_{A,\text{Surface}}$, in terms of its molar density in the bulk gas phase, $C_{A,\text{BulkGas}}$. The final result is

$$k_{A,\text{MTC}}(C_{A,\text{BulkGas}} - C_{A,\text{Surface}})S_{\text{external}} = ES_m\rho_{\text{apparent}}R_{\text{Surface}}(C_{A,\text{Surface}})V_{\text{catalyst}} \tag{22}$$

where V_{catalyst} and S_{external} represent the volume and external surface area, respectively, of one catalytic pellet. The presence of the effectiveness factor on

the right side of the previous equation indicates that the rate of consumption of reactant A is averaged volumetrically throughout the pellet. It is not sufficient to evaluate the kinetic rate law on the external surface of a porous catalyst without including the effectiveness factor.

2.5. Dimensionless Mass Transfer Equation for Steady-State Analysis of Ideal and Nonideal Packed Catalytic Tubular Reactors. Begin with a plug-flow version of the mass balance for key reactant A, where the important independent variable (ie, z-direction in cylindrical coordinates) increases in the direction of flow of the reactive mixture. When the bulk-gas molar density of reactant A is dimensionalized by its value at the tube inlet (ie, $z = 0^-$, $C_{A,\mathrm{BulkGas}} = C_{A,\mathrm{inlet}}$)

$$\Psi_{A,\mathrm{BulkGas}} = \frac{C_{A,\mathrm{BulkGas}}}{C_{A,\mathrm{inlet}}} = \frac{C_{A,\mathrm{BulkGas}}}{C_{A,\mathrm{BulkGas}}(z = 0^-)} \tag{23}$$

the following dimensionless equation is appropriate to simulate nonideal reactor performance (2). The important mass transfer rate processes are convection (ie, first-derivative term on the left side of eq. 24), interpellet axial dispersion (ie, second-derivative term on the right side of eq. 24), and one pseudo-volumetric nth-order irreversible chemical reaction on the internal surface of porous catalysts (ie, second-term on the right side of eq. 24). The rate law depends only on the molar density of reactant A, whose stoichiometric coefficient is -1.

$$Pe_{MT}\frac{d}{d\zeta_{\mathrm{PFR}}}\Psi_{A,\mathrm{BulkGas,Real}} = \frac{d^2}{d\zeta_{\mathrm{PFR}}^2}\Psi_{A,\mathrm{BulkGas,Real}} - \Lambda_{A,\mathrm{interpellet}}^2(1 - \varepsilon_{p,\mathrm{interpellet}})E\Psi_{A,\mathrm{Surface,Real}}^n \tag{24}$$

where $\zeta_{\mathrm{PFR}} = z/L_{\mathrm{PFR}}$ is the dimensionless independent variable in the primary flow direction. The mass transfer Peclet number Pe_{MT} (ie, product of the Reynolds and Schmidt numbers), also known as the *vessel Peclet number* (4), represents an *order-of-magnitude* estimate of the rate of convective mass transfer relative to the rate of interpellet axial dispersion. Pe_{MT} contains the interstitial fluid velocity, based on volumetric flowrate q and the cross-sectional area available for flow, as well as the interpellet axial dispersion coefficient $D_{A,\mathrm{interpellet}}$ for reactant A.

$$Pe_{MT} = \frac{qL_{\mathrm{PFR}}}{\varepsilon_{p,\mathrm{interpellet}}\pi R_{\mathrm{PFR}}^2 D_{A,\mathrm{interpellet}}} \tag{25}$$

The interpellet Damköhler number represents a dimensionless ratio of the pseudo-volumetric rate of the nth-order chemical reaction relative to the rate of interpellet axial dispersion, and it contains the characteristic molar density of reactant A in the inlet stream when $n \neq 1$, as well as reactor length L_{PFR}, which represents the characteristic length for this one-dimensional problem in cylindrical coordinates. If $S_m\rho_{\mathrm{apparent}}k_{n,\mathrm{Surface}}$ is a temperature-dependent nth-order pseudo-volumetric kinetic rate constant, with dimensions of $(\mathrm{volume/mol})^{n-1}$

per time, for pseudo-volumetric rates of reaction (ie, dimensions of moles per pellet volume per time) that are expressed using molar densities on the external surface of the catalyst, then the interpellet Damköhler number for reactant A is defined as

$$\Lambda^2_{A,\text{interpellet}} = \frac{S_m \rho_{\text{apparent}} k_{n,\text{Surface}} L^2_{\text{PFR}} C^{n-1}_{A,\text{inlet}}}{D_{A,\text{interpellet}}} \tag{26}$$

Homogeneous chemical reactions in nonideal tubular reactors (ie, empty tubes) that contain no porous catalytic pellets are described by a very similar plug-flow mass balance (see eq. 24), except (*1*) the interpellet porosity (ie, void volume fraction) of the packed bed, $\varepsilon_{p,\text{interpellet}}$, and the effectiveness factor E should be omitted from the differential mass and thermal energy balances; (*2*) the kinetic rate law requires the bulk molar density of reactant A, instead of its molar density on the external surface of the catalyst; and (*3*) the mass transfer Peclet number and the interpellet Damköhler number contain the ordinary molecular diffusion coefficient of species A, instead of the interpellet axial dispersion coefficient in the denominator of each dimensionless number (4,5). Ideal reactor performance with either homogeneous or heterogeneous chemical kinetics can be simulated by excluding the second-derivative term on the right side of equation 24, because either ordinary molecular diffusion in the flow direction of *empty tubes* or interpellet axial dispersion in packed beds does not affect reactant conversion in the exit stream. Ideal reactor modeling is justified when the mass transfer Peclet number exceeds its critical value (see Section 2.7). In heterogeneous packed catalytic tubular reactors, reactants are converted to products via chemical reaction on the internal surface of the catalyst. Volumetric averaging of the rate of reactant consumption within porous catalysts is addressed by (*1*) evaluating the kinetic rate law using molar densities on the external surface of the catalyst and (*2*) including the effectiveness factor in the plug-flow mass and thermal energy balances. The factor of $(1-\varepsilon_{p,\text{interpellet}})$ in the dimensionless rate law of equation 24 corresponds to the ratio of pellet volume to total reactor volume. It is required in the differential plug-flow mass and thermal energy balances because

(1) $ES_m \rho_{\text{apparent}} R_{\text{Surface}}(C_{A,\text{Surface}})$ represents an average, over the volume of each pellet, of the pseudo-volumetric rate of reactant consumption, with units of moles *per volume of catalyst* per time.
(2) Plug-flow balances are based on a differential control volume for the entire packed catalytic tubular reactor (ie, $dV_{\text{Reactor}} = \pi R^2{}_{\text{PFR}} dz$).
(3) Hence, the volumetrically averaged rate of reactant consumption throughout the catalyst, with units of moles per time, is manipulated as follows:

$$ES_m \rho_{\text{apparent}} R_{\text{Surface}} dV_{\text{pellet}} = ES_m \rho_{\text{apparent}} R_{\text{Surface}} (1 - \varepsilon_{p,\text{interpellet}}) dV_{\text{Reactor}} \tag{27}$$

because $V_{\text{pellet}} = (1-\varepsilon_{p,\text{interpellet}}) V_{\text{Reactor}}$. The product of ρ_{apparent} and $(1-\varepsilon_{p,\text{interpellet}})$ is equivalent to the density of the entire packed bed. The

minimum interpellet porosity, or minimum void volume fraction of the packed bed, is 26% for hexagonal-close-packed and cubic-close-packed arrangements of spherical pellets. One final step in developing the plug-flow mass and thermal energy balances is division by the size of the differential control volume, dV_{Reactor}.

2.6. Zeroth-Order Chemical Kinetics in Packed Catalytic Tubular Reactors, with and without Interpellet Axial Dispersion: The Danckwerts Boundary Conditions. Consider the differential design equation for packed catalytic tubular reactors with zeroth-order chemical kinetics. When interpellet axial dispersion is negligible at large mass transfer Peclet numbers, one must solve the following first-order ordinary differential equation (ie, ODE):

$$Pe_{MT}\frac{d\Psi_{A,\text{BulkGas,Ideal}}}{d\zeta_{\text{PFR}}} = -E(\Lambda_{A,\text{intrapellet}})\{1-\varepsilon_{p,\text{interpellet}}\}\Lambda^2_{A,\text{interpellet}} \tag{28}$$

subject to the boundary condition that the dimensionless molar density $\Psi_{A,\text{BulkGas,Ideal}}$ of reactant A under ideal conditions is, by definition, unity at the reactor inlet where $\zeta_{\text{PFR}} = 0$. As the reaction rate is independent of molar density for zeroth-order chemical kinetics, equation 28 is valid for ideal tubular reactors in which external mass transfer resistance is included or neglected, provided that the catalytic surface is not starved of reactants. If the product of the effectiveness factor, the catalyst filling factor, and the interpellet Damköhler number on the right side of equation 28 is denoted by Ω (ie, the *chemical reaction coefficient*).

$$\Omega = E(\Lambda_{A,\text{intrapellet}})\{1-\varepsilon_{p,\text{interpellet}}\}\Lambda^2_{A,\text{interpellet}} \tag{29}$$

then the solution to equation 28 is

$$\Psi_{A,\text{BulkGas,Ideal}} = 1 - \left\{\frac{\Omega}{Pe_{MT}}\right\}\zeta_{\text{PFR}} \tag{30}$$

When interpellet axial dispersion is important at low mass transfer Peclet numbers, the differential design equation for nonideal reactors corresponds to a second-order ODE.

$$\begin{aligned} Z &= \frac{d\Psi_{A,\text{BulkGas,Real}}}{d\zeta_{\text{PFR}}} \\ \frac{dZ}{d\zeta_{\text{PFR}}} &= Pe_{MT}Z + E(\Lambda_{A,\text{intrapellet}})\{1-\varepsilon_{p,\text{interpellet}}\}\Lambda^2_{A,\text{interpellet}} \end{aligned} \tag{31}$$

The homogeneous analytical solution for the dimensionless axial reactant concentration gradient in nonideal reactors is

$$Z_{\text{homogeneous}} = \left\{\frac{d\Psi_{A,\text{BulkGas,Real}}}{d\zeta_{\text{PFR}}}\right\}_{\text{homogeneous}} = C_1\exp(Pe_{MT}\zeta_{\text{PFR}}) \tag{32}$$

The particular solution, which is the same as the complete axial concentration gradient in ideal packed catalytic tubular reactors with zeroth-order kinetics, is

$$Z_{\text{particular}} = \left\{\frac{d\Psi_{A,\text{BulkGas,Real}}}{d\zeta_{\text{PFR}}}\right\}_{\text{particular}} = -\frac{\Omega}{Pe_{MT}} \tag{33}$$

The Danckwerts boundary condition in the exit stream (ie, $Z \Rightarrow 0$ when $\zeta_{\text{PFR}} \Rightarrow 1$) is satisfied when

$$C_1 = \frac{\Omega}{Pe_{MT}} \exp(-Pe_{MT}) \tag{34}$$

The final expression for the dimensionless axial reactant concentration gradient in nonideal reactors is obtained by adding the homogeneous and particular solutions for Z, given by equations 32 and 33, respectively.

$$Z = \left\{\frac{d\Psi_{A,\text{BulkGas,Real}}}{d\zeta_{\text{PFR}}}\right\} = -\frac{\Omega}{Pe_{MT}}\{1 - \exp[-Pe_{MT}(1 - \zeta_{\text{PFR}})]\} \tag{35}$$

Equation 35 is integrated analytically to obtain the molar density profile of reactant A for zeroth-order chemical kinetics in nonideal packed catalytic tubular reactors in which interpellet axial dispersion is important. If the catalytic surface is not starved of reactants, then the following expression is valid when external mass transfer resistance is either included or neglected because reactant molar density does not appear in the rate law for zeroth-order kinetics:

$$\Psi_{A,\text{BulkGas,Real}}(\zeta_{\text{PFR}}) = C_2 - \frac{\Omega}{Pe_{MT}}\left\{\zeta_{\text{PFR}} - \frac{1}{Pe_{MT}}[\{\exp(Pe_{MT}\zeta_{\text{PFR}}) - 1\}\exp(-Pe_{MT})]\right\} \tag{36}$$

The boundary condition at the reactor inlet governs the value of integration constant C_2 in equation 36. For example, if one employs the definition of dimensionless reactant molar density, which requires that $\Psi_{A,\text{BulkGas,Real}} = 1$ at $\zeta_{\text{PFR}} = 0$, then $C_2 = 1$. However, the Danckwerts boundary condition at the reactor inlet (4,6) (see the discussion of eq. 51) suggests that

$$\Psi_{A,\text{BulkGas,Real}}(\zeta_{\text{PFR}} = 0) - \frac{1}{Pe_{MT}}\left\{\frac{d\Psi_{A,\text{BulkGas,Real}}}{d\zeta_{\text{PFR}}}\right\}_{\zeta_{\text{PFR}}=0} = 1 \tag{37}$$

Now

$$C_2 = 1 - \frac{\Omega}{Pe_{MT}^2}\{1 - \exp(-Pe_{MT})\} \tag{38}$$

The final expression for the reactant molar density profile, which satisfies Danckwerts boundary conditions at the inlet and outlet, is given by equations 36 and 38;

$$\Psi_{A,\mathrm{BulkGas,Real}}(\zeta_{\mathrm{PFR}}) = \Psi_{A,\mathrm{BulkGas,Ideal}}(\zeta_{\mathrm{PFR}}) - \frac{\Omega}{Pe_{MT}^2}\{1 - \exp[-Pe_{MT}(1 - \zeta_{\mathrm{PFR}})]\} \tag{39}$$

If one evaluates equations 30, 36, and 39 in the exit stream (ie, $\zeta_{\mathrm{PFR}} = 1$) and compares the final conversion of reactant A {ie, $1 - \Psi_{A,\mathrm{BulkGas}}(\zeta_{\mathrm{PFR}} = 1)$} for real and ideal packed catalytic tubular reactors with zeroth-order chemical kinetics, then the following results are obtained:

(1) If $\Omega \leq Pe_{MT}$, then Ω/Pe_{MT} represents the conversion that one should achieve under ideal conditions via equation 30 when the mass transfer Peclet number is larger than its critical value, such that interpellet axial dispersion is negligible. Reactants have not been consumed completely, and mass transfer resistance between the bulk fluid phase and the external surface of the catalyst is not an important factor for reactor design.

(2) Equation 39 indicates that *nonideal* reactors that satisfy both Danckwerts boundary conditions achieve the same final conversion that is predicted by the ideal design equation.

(3) Equation 36 suggests that *nonideal* reactors that satisfy the Danckwerts boundary condition in the exit stream and the ideal reactor boundary condition at the inlet, (C_2 = 1), based on the definition of dimensionless reactant molar density, achieve less conversion than ideal reactors, because $\Psi_{A,\mathrm{BulkGas,Real}}(\zeta_{\mathrm{PFR}} = 1)$ is larger than $\Psi_{A,\mathrm{BulkGas,Ideal}}(\zeta_{\mathrm{PFR}} = 1)$.

$$\Psi_{A,\mathrm{BulkGas,Real}}(\zeta_{\mathrm{PFR}} = 1) = \Psi_{A,\mathrm{BulkGas,Ideal}}(\zeta_{\mathrm{PFR}} = 1) + \frac{\Omega}{Pe_{MT}^2}\{1 - \exp(-Pe_{MT})\} \tag{40}$$

When the mass transfer Peclet number is *large enough* (ie, larger than its critical value that increases at higher interpellet Damköhler numbers; see equation 43 and Table 1), the second term on the right side of equation 40 is negligible and the PFR behaves ideally.

2.7. Critical Value of the Mass Transfer Peclet Number, Below Which Interpellet Axial Dispersion Must be Included in Nonideal Tubular Reactor Models. Simulations are compared for ideal and nonideal tubular reactors under isothermal conditions in the absence of external mass transfer resistance. The kinetics are nth-order irreversible, with $n = 1$ or 2, and the bulk gas-phase molar density of reactant A is sufficient to evaluate the rate law when external mass transfer resistance is negligible. In light of results from the previous section, both types of reactors obey ideal PFR boundary conditions at the inlet, whereas nonideal reactors satisfy the Danckwerts boundary condition in the exit stream. The following problems are analyzed for given values of Ω, which is described as the *chemical reaction coefficient*, and the mass transfer Peclet number is increased

Table 1. **Effect of the Chemical Reaction Coefficient Ω on the Critical Value of the Mass Transfer Peclet Number for Simple *n*th-Order Irreversible Chemical Kinetics in Packed Catalytic Tubular Reactors**

$\Omega = \Lambda^2_{A,\text{interpellet}}(1-\varepsilon_{p,\text{interpellet}})E$	$(\text{Re}Sc)_{\text{critical}}$, $n = 1$	$(\text{Re}Sc)_{\text{critical}}$, $n = 2$
0.5		10
1	15	15
2	21	
4	30	
5	34	30
7	40	
10	49	50
15	61	
20	71	
25	80	
30	89	
40	104	
50	118	90
75	149	105
100	176	115

Interpellet axial dispersion does not affect reactor performance when Pe_{MT} exceeds $(\text{Re}Sc)_{\text{critical}}$.

systematically until it achieves its critical value when both solutions for the bulk gas-phase molar density of key reactant A in the exit stream are indistinguishable. The ideal reactor is described by a first-order ODE (ie, eq. 24 without the second-derivative term) that can be solved analytically for any value of n.

$$\begin{aligned} Pe_{MT}\frac{d\Psi_{A,\text{BulkGas,Ideal}}}{d\zeta_{\text{PFR}}} &= -\Lambda^2_{A,\text{interpellet}}\{1-\varepsilon_{p,\text{interpellet}}\}E\Psi^n_{A,\text{BulkGas,Ideal}} \\ &= -\Omega\Psi^n_{A,\text{BulkGas,Ideal}} \\ \Psi_{A,\text{BulkGas,Ideal}}(\zeta_{\text{PFR}}=0) &= 1 \\ \Psi_{A,\text{BulkGas,Ideal}}(\zeta_{\text{PFR}}=1;n=1) &= \exp\left\{-\frac{\Omega}{Pe_{MT}}\right\} \\ \Psi_{A,\text{BulkGas,Ideal}}(\zeta_{\text{PFR}}=1;n\neq 1) &= \left\{\frac{Pe_{MT}}{Pe_{MT}+(n-1)\Omega}\right\}^{1/(n-1)} \end{aligned} \tag{41}$$

Nonideal reactors are described by one second-order ODE (ie, eq. 24) that can be written as two coupled first-order ODEs with split boundary conditions (2).

$$\begin{aligned} Z &= \frac{d\Psi_{A,\text{BulkGas,Real}}}{d\zeta_{\text{PFR}}} \\ \frac{dZ}{d\zeta_{\text{PFR}}} &= Pe_{MT}Z + \Lambda^2_{A,\text{interpellet}}\{1-\varepsilon_{p,\text{interpellet}}\}E\Psi^n_{A,\text{BulkGas,Real}} \\ &= Pe_{MT}Z + \Omega\Psi^n_{A,\text{BulkGas,Real}} \\ \Psi_{A,\text{BulkGas,Real}}(\zeta_{\text{PFR}}=0) &= 1 \\ Z(\zeta_{\text{PFR}}=1) &\Rightarrow 0 \end{aligned} \tag{42}$$

Trial-and-error is required, because one must provide guesses for the dimensionless axial molar density gradient Z at the inlet to initiate numerical integration. The correct guess for Z at $\zeta_{\mathrm{PFR}} = 0$ yields convergence of the Danckwerts boundary condition in the exit stream. For some values of Ω and Pe_{MT}, this nonideal reactor problem is extremely sensitive to the initial guess for Z at $\zeta_{\mathrm{PFR}} = 0$. Changes in the initial guess on the order of 10^{-11} produce enormous fluctuations in reactant molar density profiles such that it is not possible to converge on the Danckwerts boundary condition in the exit stream. Some of these instabilities associated with numerical solutions of *stiff differential equations* can be avoided by (*1*) reformulating the problem such that a new independent variable is introduced, which increases from outlet to inlet, and (*2*) integrating *backwards* (7). The following trends are observed. When the kinetic rate law is simple nth-order, irreversible, and only a function of the molar density of reactant A, with $n > 0$, one achieves a higher conversion of reactants to products under ideal conditions in plug-flow tubular reactors (PFRs) relative to continuous stirred tank reactors (CSTRs). PFRs represent the extreme of no mixing, whereas CSTRs correspond to the other extreme of complete mixing. Hence, it is reasonable that when axial diffusion or interpellet axial dispersion is included in the nonideal PFR differential design equation, one achieves less conversion of reactants to products relative to ideal PFR predictions because diffusion or dispersion introduces mixing ahead of and behind the "plug." In order of decreasing outlet conversion of reactants to products, the following trend is observed: (*1*) ideal PFRs with no axial mixing, (*2*) real PFRs with some axial mixing, and (*3*) ideal CSTRs with complete mixing throughout the reactor. The mass transfer Peclet number and the reactor type govern the extent of mixing, where smaller values of Pe_{MT} in differential tubular reactors correspond to more mixing. Hence, an increase in Pe_{MT} reduces the effect of axial mixing. When the mass transfer Peclet number exceeds its critical value, interpellet axial dispersion in the nonideal reactor model has no effect on reactant conversion and simulations for both types of tubular reactors (ideal vs. nonideal) yield the same predictions. It is advantageous to document critical values of the mass transfer Peclet number $(\mathrm{Re}Sc)_{\mathrm{critical}}$ because, if one operates above the critical value, it is not necessary to include interpellet axial dispersion in the reactor model and solve two coupled first-order ODEs numerically with split boundary conditions that are sensitive to the initial guess for Z at $\zeta_{\mathrm{PFR}} = 0$. Ideal tubular reactor simulations for simple nth-order kinetics exhibit analytical solutions for any reaction order n, given by equation 41. Table 1 summarizes the effect of the chemical reaction coefficient on $(\mathrm{Re}Sc)_{\mathrm{critical}}$ for $n = 1$ and $n = 2$ in tubular reactors. If the reactor does not contain porous catalytic pellets, then the results summarized in Table 1 and equation 43 are applicable if one neglects the interpellet porosity $\varepsilon_{p,\mathrm{interpellet}}$ and the effectiveness factor E in the definition of Ω, and the mass transfer Peclet number is evaluated in terms of (*1*) the superficial fluid velocity through an empty tube and (*2*) the ordinary molecular diffusion coefficient instead of the interpellet axial dispersion coefficient. For chemical reaction coefficients Ω between 100 and 500, the following empirical equation is applicable when $n = 1$:

$$(\mathrm{Re}Sc)_{\mathrm{critical}} \approx 111 + 0.72\,\Lambda^2_{A,\mathrm{interpellet}}(1 - \varepsilon_{p,\mathrm{interpellet}})E \tag{43}$$

2.8. Design of Ideal Isothermal Packed Catalytic Tubular Reactors with First-Order Irreversible Chemical Kinetics When the External Resistance to Mass Transfer Cannot be Neglected. If the rate of thermal energy generated by exothermic chemical reactions is counterbalanced by the rate of heat removal across the outer diathermal wall, then temperature changes throughout the reactor are negligible and the thermal energy balance is not required. At high mass transfer Peclet numbers where interpellet axial dispersion is negligible and ideal tubular reactor simulations are justified, one must solve the following first-order ODE (ie, species mass balance) and supporting algebraic equation (ie, accounting for external mass transfer resistance via equation 22) when the kinetics are first-order and irreversible (ie, $n = 1$):

$$Pe_{MT}\frac{d\Psi_{A,\text{BulkGas,Ideal}}}{d\zeta_{\text{PFR}}} = -\Lambda^2_{A,\text{interpellet}}\{1-\varepsilon_{p,\text{interpellet}}\}E\Psi^n_{A,\text{Surface,Ideal}} = -\Omega\Psi^n_{A,\text{Surface,Ideal}}$$

$$k_{A,\text{MTC}}(C_{A,\text{BulkGas,Ideal}} - C_{A,\text{Surface,Ideal}})S_{\text{external}} = ES_m\rho_{\text{apparent}}k_{n,\text{Surface}}C^n_{A,\text{Surface,Ideal}}V_{\text{catalyst}}$$

$$\Psi_{A,\text{BulkGas,Ideal}}(\zeta_{\text{PFR}} = 0) = 1 \tag{44}$$

where the heterogeneous kinetic rate law, with dimensions of moles per internal catalytic surface area per time, is expressed as $R_{\text{Surface}}(C_{A,\text{Surface,Ideal}}) = k_{1,\text{Surface}}\ C_{A,\text{Surface,Ideal}}$ and $k_{1,\text{Surface}}$ is a reaction velocity constant with dimensions of length per time. Analytical integration of the plug-flow mass balance in equation 44 is not possible until one obtains explicit evaluation $C_{A,\text{Surface,Ideal}}$ in terms of $C_{A,\text{BulkGas,Ideal}}$, which is only possible for zeroth-order, first-order, and second-order kinetics. Dimensional analysis of the supporting algebraic equation, which equates the rate of mass transfer of reactant A from the bulk fluid phase toward the external surface of the catalyst and the volumetrically averaged rate of reactant consumption within porous pellets via effectiveness factor formalism, [ie, see equation 22], employs the inlet molar density of reactant A as the characteristic molar density for this problem. Hence,

$$\Psi_{A,\text{BulkGas,Ideal}} = \frac{C_{A,\text{BulkGas,Ideal}}}{C_{A,\text{Inlet}}};\ \Psi_{A,\text{Surface,Ideal}} = \frac{C_{A,\text{Surface,Ideal}}}{C_{A,\text{Inlet}}}$$

$$\Psi_{A,\text{BulkGas,Ideal}} - \Psi_{A,\text{Surface,Ideal}} = \frac{ES_m\rho_{\text{apparent}}k_{n,\text{Surface}}V_{\text{catalyst}}C^{n-1}_{A,\text{Inlet}}}{k_{A,\text{MTC}}S_{\text{external}}}\Psi^n_{A,\text{Surface,Ideal}}$$

$$\alpha = \frac{ES_m\rho_{\text{apparent}}k_{n,\text{Surface}}V_{\text{catalyst}}C^{n-1}_{A,\text{Inlet}}}{k_{A,\text{MTC}}S_{\text{external}}}$$

$$\alpha\Psi^n_{A,\text{Surface,Ideal}} + \Psi_{A,\text{Surface,Ideal}} - \Psi_{A,\text{BulkGas,Ideal}} = 0 \tag{45}$$

Equation 45 provides an algebraic relation between dimensionless bulk gas and surface molar densities of reactant A that is linear for zeroth-order

and first-order kinetics. The complete solution for $n = 1$ is given by

$$\begin{aligned}\Psi_{A,\text{Surface,Ideal}} &= \frac{1}{1+\alpha}\Psi_{A,\text{BulkGas,Ideal}} \\ \Psi_{A,\text{BulkGas,Ideal}}(\zeta_{\text{PFR}}) &= \exp\left\{-\frac{\Omega\zeta_{\text{PFR}}}{(1+\alpha)Pe_{MT}}\right\} \\ &= \exp\left\{-\frac{\Lambda^2_{A,\text{interpellet}}(1-\varepsilon_{p,\text{interpellet}})E\zeta_{\text{PFR}}}{(1+\alpha)Pe_{MT}}\right\} \end{aligned} \tag{46}$$

where α is the dimensionless parameter that governs the importance of external mass transfer resistance. In the reaction-controlled regime where α approaches zero, external mass transfer resistance is not very important and the assumption of volumetrically averaged catalytic reaction rates based on bulk gas-phase molar densities is valid. These conditions are achieved at (*1*) low rates of reactant conversion, (*2*) small catalytic pellets with large external surface-to-volume ratios, and (*3*) high gas-phase flow rates through the packed bed. Reactant conversion suffers considerably in the diffusion-controlled regime where rates of mass transfer of reactants toward the catalytic surface are much slower than reaction rates and α increases without bound. All parametric changes that increase the argument of the exponential in equation 46 for $\Psi_{A,\text{BulkGas,Ideal}}$ produce higher conversion without increasing reactor volume because, in most cases, when kinetic rate laws are evaluated at higher reactant molar densities, one achieves greater reactant-to-product conversion rates.

2.9. Isothermal Design of Ideal and Nonideal Packed Catalytic Tubular Reactors with Second-Order Irreversible Chemical Kinetics When the External Resistance to Mass Transfer is Significant. When $n = 2$ in equation 45, the quadratic formula is useful to relate surface and bulk-gas molar densities of reactant A in ideal and nonideal reactors that contain porous catalysts. Hence, for ideal and real reactor performance, one obtains the following relation between bulk and surface molar densities of reactant A for second-order irreversible chemical kinetics when the rate law depends only on $\Psi_{A,\text{Surface}}$:

$$\begin{aligned}&\alpha\Psi^2_{A,\text{Surface}} + \Psi_{A,\text{Surface}} - \Psi_{A,\text{BulkGas}} = 0 \\ &\Psi_{A,\text{Surface}} = \frac{1}{2\alpha}\{-1 + \sqrt{1 + 4\alpha\Psi_{A,\text{BulkGas}}}\}\end{aligned} \tag{47}$$

This result reduces to (*1*) $\Psi_{A,\text{Surface}} = \Psi_{A,\text{BulkGas}}$ if the external resistance to mass transfer is negligible (ie, $\alpha = 0$), and (*2*) $\Psi_{A,\text{Surface}} \Rightarrow 0$ when $\alpha \Rightarrow \infty$. Equation 47 for $\Psi_{A,\text{Surface}}$ is required for ideal and nonideal tubular reactor design because the rate of conversion of reactants to products employs molar densities on the external surface of the catalyst, together with the effectiveness factor. The performance of ideal plug-flow tubular reactors with second-order irreversible chemical kinetics and significant

external mass transfer resistance is described by the following equations for $\Psi_{A,\mathrm{BulkGas,Ideal}}$:

$$\begin{aligned} Pe_{MT}\frac{d\Psi_{A,\mathrm{BulkGas,Ideal}}}{d\zeta_{\mathrm{PFR}}} &= -\Lambda^2_{A,\mathrm{interpellet}}\{1-\varepsilon_{p,\mathrm{interpellet}}\}E\Psi^2_{A,\mathrm{Surface,Ideal}} \\ &= -\Omega\Psi^2_{A,\mathrm{Surface,Ideal}} \\ \Psi_{A,\mathrm{BulkGas,Ideal}}(\zeta_{\mathrm{PFR}}=0) &= 1 \end{aligned} \tag{48}$$

When interpellet axial dispersion is important at low mass transfer Peclet numbers, the following set of coupled first-order ODEs must be analyzed together to calculate $\Psi_{A,\mathrm{BulkGas,Real}}$:

$$\begin{aligned} Z &= \frac{d\Psi_{A,\mathrm{BulkGas,Real}}}{d\zeta_{\mathrm{PFR}}} \\ \frac{dZ}{d\zeta_{\mathrm{PFR}}} &= Pe_{MT}Z + \Lambda^2_{A,\mathrm{interpellet}}\{1-\varepsilon_{p,\mathrm{interpellet}}\}E\Psi^2_{A,\mathrm{Surface,Real}} \\ &= Pe_{MT}Z + \Omega\Psi^2_{A,\mathrm{Surface,Real}} \\ \Psi_{A,\mathrm{BulkGas,Real}}(\zeta_{\mathrm{PFR}}=0) &= 1 \\ Z(\zeta_{\mathrm{PFR}}=1) &\Rightarrow 0 \end{aligned} \tag{49}$$

In "closed-closed" tubular reactors with no axial dispersion or radial variations in molar density upstream and downstream from the packed section of catalytic pellets, Bischoff (8) proved rigorously that the Danckwerts boundary condition (9) at the reactor inlet is

$$\Psi_{A,\mathrm{BulkGas,Real}}(\zeta_{\mathrm{PFR}}=0) - \frac{1}{Pe_{MT}}\left\{\frac{d}{d\zeta_{\mathrm{PFR}}}\Psi_{A,\mathrm{BulkGas,Real}}\right\}_{\zeta_{\mathrm{PFR}}=0} = 1 \tag{50}$$

which was also employed by Irving Langmuir (10). One arrives at equation 50 by invoking continuity of the rate of mass transfer of reactant A at $\zeta_{\mathrm{PFR}}=0^-$ and $\zeta_{\mathrm{PFR}}=0^+$, where interpellet axial dispersion exists within the packed bed, but not upstream from the inlet where the catalytic pellets are absent and no chemical reaction occurs. The cross-sectional area for fluid flow decreases abruptly at the inlet, with a corresponding increase in average fluid velocity at the same volumetric flowrate q due to the presence of the catalytic pellets. Hence, continuity of the rate of mass transfer for reactant A at $z=0$ yields the following *dimensional* Danckwerts boundary condition at the reactor inlet:

$$\begin{aligned} qC_{A,\mathrm{BulkGas,Real}}(z=0^-) &= qC_{A,\mathrm{BulkGas,Real}}(z=0^+) \\ &\quad - D_{A,\mathrm{interpellet}}\left\{\frac{d}{dz}C_{A,\mathrm{BulkGas,Real}}\right\}_{z=0^+}\pi R^2_{\mathrm{PFR}}\varepsilon_{p,\mathrm{interpellet}} \\ q = \pi R^2_{\mathrm{PFR}}\langle v_z\rangle_{\mathrm{superficial}} &= \varepsilon_{p,\mathrm{interpellet}}\pi R^2_{\mathrm{PFR}}\langle v_z\rangle_{\mathrm{interstitial}} \end{aligned} \tag{51}$$

The characteristic molar density required for dimensional analysis is $C_{A,\mathrm{BulkGas,Real}}(z=0^-)$, and $z=\zeta_{\mathrm{PFR}}L_{\mathrm{PFR}}$. Even though chemical reaction occurs beyond the inlet, but it is absent prior to the inlet, division of the steady-state balance for reactant A at $z=0$ (ie, eq. 51) by the product of the volumetric flowrate q and $C_{A,\mathrm{BulkGas,Real}}(z=0^-)$ yields the required Danckwerts boundary condition at the inlet (ie, eq. 50), where the mass transfer Peclet number Pe_{MT} contains the interstitial fluid velocity, reactor length L_{PFR}, and the interpellet axial dispersion coefficient $D_{A,\mathrm{interpellet}}$ (see eq. 25 for the definition of Pe_{MT}). Hiby (11) has demonstrated that there is no true "back mixing" in packed beds, and Wicke (12) suggests that molecular diffusion across the inlet plane at $\zeta_{\mathrm{PFR}}=0$ is negligible even at small mass transfer Peclet numbers. Hence, it is reasonable to invoke continuity of reactant conversion and let $\Psi_{A,\mathrm{BulkGas,Real}}=1$ at $\zeta_{\mathrm{PFR}}=0$ in packed catalytic tubular reactors, realizing that all possible boundary conditions at the reactor inlet yield similar results at high mass transfer Peclet numbers. Instabilities arise during numerical integration of two coupled ODEs which describe steady-state convection, interpellet axial dispersion, and nth-order irreversible chemical reaction for certain combinations of interpellet Damköhler numbers and mass transfer Peclet numbers (7). Hence, it might be best to guess the outlet bulk molar density of reactant A and integrate the nonideal plug-flow mass transfer equation (ie, eq. 49) backward from outlet to inlet, until convergence is obtained at $\zeta_{\mathrm{PFR}}=0$, where $\Psi_{A,\mathrm{BulkGas,Real}}=1$. This is accomplished in practice by (*1*) defining a new independent spatial variable $\xi_{\mathrm{PFR}}=1-\zeta_{\mathrm{PFR}}$, which increases as one moves toward the reactor inlet, and (*2*) introducing a negative sign in each term on the right side of both coupled first-order ODEs that represent the one-dimensional mass balance (ie, eq. 49). Simulation of this problem in ideal and real tubular reactors is provided in tabular form (see Table 2) after α is evaluated in terms of the other dimensionless numbers of interest in mass transfer. In other words, α cannot be chosen independently for each reactor simulation.

Table 2. **Effect of the Mass Transfer Peclet Number on Dimensionless Reactant Molar Densities in the Bulk Fluid Phase and Near the External Surface of Catalytic Pellets in Real and Ideal Heterogeneous Packed Catalytic Tubular Reactors, with and without (ie, $\alpha=0$) Significant External Mass Transfer Resistance**

Pe_{MT}	0.5	1	2	3	6	8	10
α	90.5	22.6	5.66	2.51	0.628	0.353	0.226
$\Psi_{A,\mathrm{Surface}}(\zeta=0)$	0.0997	0.189	0.341	0.462	0.696	0.783	0.840
$\Psi_{A,\mathrm{Surface,Ideal}}(\zeta=1)$	0.0947	0.172	0.287	0.370	0.523	0.588	0.638
$\Psi_{A,\mathrm{BulkGas,Ideal}}(\zeta=1)$	0.905	0.837	0.754	0.713	0.694	0.710	0.730
$\Psi_{A,\mathrm{BulkGas,Ideal}}(\zeta=1;\alpha=0)$	0.091	0.167	0.286	0.375	0.545	0.615	0.667
$-(d\Psi_{A,\mathrm{BulkGas,Real}}/d\zeta)_{\zeta=0}$	0.0385	0.1086	0.2316	0.3061	0.3689	0.3576	0.3341
$\Psi_{A,\mathrm{Surface,Real}}(\zeta=1)$	0.0986	0.183	0.311	0.400	0.554	0.615	0.661
$\Psi_{A,\mathrm{BulkGas,Real}}(\zeta=1)$	0.979	0.937	0.856	0.801	0.747	0.749	0.760
$\Psi_{A,\mathrm{BulkGas,Real}}(\zeta=1;\alpha=0)$	0.424	0.447	0.489	0.528	0.620	0.666	0.703

The other important dimensionless numbers that govern reactor performance are $\Omega=5$, $Pe_{\mathrm{particle}}=50$, $\{\mathrm{Re}Sc\}_{\mathrm{critical}}=30$, $\varphi_{\mathrm{correlation}}=1$, $\varepsilon_{p,\mathrm{interpellet}}=0.5$, $n=2$ (reaction order). The chemical kinetics are second-order and irreversible.

2.10. Important Dimensionless Parameter that Governs the Significance of External Mass Transfer Resistance. The important dimensionless parameter that determines the significance of external mass transfer resistance for *n*th-order irreversible chemical kinetics in packed catalytic tubular reactors is manipulated such that α can be written in terms of the *chemical reaction coefficient* Ω, the mass transfer Peclet number Pe_{MT}, and a few other dimensionless numbers that influence the design of chemical reactors. For example, the numerator of α contains $S_m \rho_{\text{apparent}} k_{n,\text{Surface}} \{C_{A,\text{inlet}}\}^{n-1}$ (see eq. 45), which also appears in the numerator of the chemical reaction coefficient via the interpellet Damköhler number. Hence, simple algebraic manipulation of equations 26,29, and 45 yields

$$\alpha = \left\{\frac{V_{\text{catalyst}}}{S_{\text{external}}}\right\} \frac{\Omega D_{A,\text{interpellet}}}{k_{A,\text{MTC}} L_{\text{PFR}}^2 (1 - \varepsilon_{p,\text{interpellet}})} \tag{52}$$

Interphase mass transfer of reactant *A* in the gas phase boundary layer external to a packed bed of porous solids has been characterized experimentally (13) and theoretically for creeping flow around an isolated solid sphere (2,13). In each case, the surface-averaged Nusselt number for mass transfer, or the particle-based Sherwood number $Sh_{\text{Average,particle}}$, scales as the one-third power of the particle-based mass transfer Peclet number Pe_{particle} for creeping flow adjacent to high-shear no-slip interfaces, where both dimensionless numbers contain the equivalent diameter of a single pellet (ie, $d_{\text{equivalent}} = 6V_{\text{catalyst}}/S_{\text{external}}$) and the ordinary molecular diffusion coefficient instead of the interpellet axial dispersion coefficient. Hence,

$$Sh_{\text{Average,particle}} = \frac{k_{A,\text{MTC}}}{D_{A,\text{ordinary}}} \left\{\frac{6V_{\text{catalyst}}}{S_{\text{external}}}\right\} \approx 2 + C_1 Pe_{\text{particle}}^{1/3} \tag{53}$$

where the coefficient of proportionality C_1 is very close to unity, the leading term (ie, 2) from stagnant film theory is negligible relative to the flow-related term, and the particle-based mass transfer Peclet number, which contains the particle-based Reynolds number, is defined in terms of the *interstitial* fluid velocity. Use of equation 53 for interphase mass transfer in packed columns is valid when the product of the particle-based Reynolds number and the interpellet porosity of the packed bed (13) is less than 20, where the Re_{particle} contains the equivalent diameter of a single catalytic pellet. Further simplification of equation 52 yields

$$\alpha \approx 6 \left\{\frac{V_{\text{catalyst}}}{L_{\text{PFR}} S_{\text{external}}}\right\}^2 \frac{\Omega}{Pe_{\text{particle}}^{1/3} (1 - \varepsilon_{p,\text{interpellet}})} \left\{\frac{D_{A,\text{interpellet}}}{D_{A,\text{ordinary}}}\right\} \tag{54}$$

Now, it is necessary to discuss experimental correlations for *flow through porous media* that allow one to calculate interpellet axial dispersion coefficients. In *Porous Media; Fluid Transport and Pore Structure* by Dullien (14), graphical results contain 175 data points for one-dimensional flow in packed beds and porous media from several different studies that encompass a wide range of particle

sizes. For particle-based mass transfer Peclet numbers between 1 and 3×10^6, experimental data were analyzed by comparing one-dimensional axial dispersion in packed beds with two-dimensional Taylor dispersion of tracers in capillary tubes. Results are summarized below with assistance from a correlation coefficient $\varphi_{\text{correlation}}$:

$$\frac{D_{A,\text{interpellet}}}{D_{A,\text{ordinary}}} \approx \varphi_{\text{correlation}} \frac{\langle v_z \rangle_{\text{interstitial}}}{D_{A,\text{ordinary}}} \left\{ \frac{6V_{\text{catalyst}}}{S_{\text{external}}} \right\} = \varphi_{\text{correlation}} Pe_{\text{particle}}$$
$$\varphi_{\text{correlation}} = \left\{ \begin{array}{l} 1; 1 \le Pe_{\text{particle}} \le 10^2 \\ 2; 10^2 < Pe_{\text{particle}} \le 3 \times 10^6 \end{array} \right\} \tag{55}$$

Explicit evaluation of interpellet axial dispersion coefficients from the previous empirical experimental correlation provides a straightforward approach to calculate vessel-based mass transfer Peclet numbers Pe_{MT}, where reactor length L_{PFR} is the characteristic distance.

$$D_{A,\text{interpellet}} \approx \varphi_{\text{correlation}} \frac{q}{\varepsilon_{p,\text{interpellet}} \pi R_{\text{PFR}}^2} \left\{ \frac{6V_{\text{catalyst}}}{S_{\text{external}}} \right\}$$
$$Pe_{MT} = \frac{qL_{\text{PFR}}}{\varepsilon_{p,\text{interpellet}} \pi R_{\text{PFR}}^2 D_{A,\text{interpellet}}} \approx \frac{L_{\text{PFR}}}{\varphi_{\text{correlation}}} \left\{ \frac{S_{\text{external}}}{6V_{\text{catalyst}}} \right\} \tag{56}$$

Equation 56 allows one to replace $V_{\text{catalyst}}/\{L_{\text{PFR}} S_{\text{external}}\}$ by $1/Pe_{MT}$ in equation 54 for α. The final result is

$$\alpha \approx \frac{\Omega Pe_{\text{particle}}^{2/3}}{6\varphi_{\text{correlation}} Pe_{MT}^2 (1 - \varepsilon_{p,\text{interpellet}})} \tag{57}$$

Simulations are given in Table 2 as a function of Pe_{MT}, when Ω and Pe_{particle} remain constant, illustrating how the outlet conversion in real and ideal packed catalytic tubular reactors with significant external mass transfer resistance (ie, $\alpha \neq 0$) is governed by competing effects that depend on the mass transfer Peclet number (2).

For example, in Table 2, the dimensionless outlet molar density of reactant A decreases and conversion increases as Pe_{MT} increases from 0.5 to 6, when the chemical reaction coefficient, which contains the interpellet Damköhler number, remains constant and $\alpha \neq 0$. When Pe_{MT} is greater than 6, the molar density of reactant A in the exit stream increases. Based on equations 25 and 26, the ratio of the interpellet Damköhler number to Pe_{MT} scales linearly with residence time τ, which decreases as one moves from left to right in Table 2. Under these conditions in the absence of external mass transfer resistance, one achieves less conversion of reactants to products because residence time decreases. This trend is observed for the dimensionless outlet molar density of reactant A in ideal and

nonideal tubular reactors for all mass transfer Peclet numbers when $\alpha = 0$. However, the external resistance to mass transfer cannot be neglected at low values of Pe_{MT}. The large difference between reactant molar densities in the bulk gas stream and those on the external surface of the catalytic pellets supports this claim. Reactor performance is extremely poor at very small Pe_{MT} because kinetic rate laws are evaluated at low surface molar densities of the reactants. This problem in the design of packed catalytic tubular reactors is corrected, to some extent, when Pe_{MT} increases, because α decreases and the external resistance to mass transfer becomes less significant. Hence, one achieves higher conversion of reactants to products at *shorter* residence times, over a restricted range of Pe_{MT} in the creeping flow regime, because α scales as $(Pe_{MT})^{-2}$, whereas τ scales as $(Pe_{MT})^{-1}$. As one moves from left to right in Table 2 at very small values of Pe_{MT}, the external resistance to mass transfer decreases more abruptly than τ decreases, and the thickness of the gas-phase mass transfer boundary layer governs the performance of packed catalytic tubular reactors. At larger values of Pe_{MT} where α is relatively small and external resistance is not very important, reactor performance is governed by the convective mass transfer rate process. Now, the primary consequence of an increase in Pe_{MT} is that τ decreases, and one achieves less conversion of reactants to products. Simulations in Table 2 reveal that the highest conversion of reactants to products is achieved in ideal PFRs with no external mass transfer resistance (ie, $\alpha = 0$). However, all simulations in Table 2 for ideal tubular reactors are not justified because one is operating at mass transfer Peclet numbers that are three-fold to sixty-fold smaller than $\{\mathrm{Re}Sc\}_{\mathrm{critical}}$. The only valid simulations in Table 2 are those that include interpellet axial dispersion and external mass transfer resistance, because $Pe_{MT} < \{\mathrm{Re}Sc\}_{\mathrm{critical}}$ and reactant molar densities near the external surface of the catalytic pellets are significantly less than those in the bulk fluid phase. In general, external resistance to mass transfer (*1*) reduces reactant molar densities on the catalytic surface, (*2*) decreases the rate of conversion of reactants to products, and (*3*) requires longer PFRs to achieve the same final conversion relative to the case where $\alpha = 0$.

2.11. Maximum Conversion in Nonideal Packed Catalytic Tubular Reactors under Isothermal Conditions with First-Order Irreversible Chemical Kinetics and Significant External Mass Transfer Resistance. Quantitative results in Table 2 reveal that one achieves maximum conversion of reactants to products (ie, $\approx 25\%$) in nonideal packed catalytic tubular reactors when $Pe_{MT} = 6$ for second-order irreversible chemical kinetics with $\Omega = 5$, $Pe_{\mathrm{particle}} = 50$, and an interpellet porosity of 50%. Hence, optimum reactor performance, which yields maximum conversion of reactants to products, might occur under nonideal conditions when external mass transfer resistance is significant. The results presented in Table 3 summarize the dependence of Pe_{MT} on the particle-based mass transfer Peclet number and the chemical reaction coefficient for first-order irreversible chemical kinetics, such that one achieves maximum conversion of reactants to products (2). In each case, the critical value of the mass transfer Peclet number is included in Table 3 to emphasize the fact that all 18 values of Pe_{MT}, where maximum conversion occurs are subcritical, requiring the inclusion of interpellet axial dispersion in these design simulations. Furthermore, the volumetrically averaged rate of conversion of reactants to products must be calculated using molar densities near the external surface of the catalytic pellets, not molar

Table 3. **Combinations of the Chemical Reaction Coefficient Ω, $Pe_{particle}$, and Pe_{MT} that Yield Maximum Conversion of Reactants to Products in Nonideal Packed Catalytic Tubular Reactors with First-Order Irreversible Chemical Kinetics (ie, $n = 1$) and external mass transfer resistance ($\varepsilon_{p,interpellet} = 0.5$)**

$\Omega = 1$ $Pe_{particle}$	$\{ReSc\}_{critical} = 15$ φ correlation	Pe_{MT}	Maximum Conversion (%)	α
1	1	1.5	23	0.15
10	1	2.0	18	0.39
50	1	3.2	14	0.44
100	1	3.7	12	0.52
250	2	4.7	10	0.30
500	2	5.7	8	0.32
$\Omega = 20$ $Pe_{particle}$	$\{ReSc\}_{critical} = 71$ φ correlation	Pe_{MT}	Maximum Conversion (%)	α
1	1	5	85	0.27
10	1	8	73	0.48
50	1	11	59	0.75
100	1	14	52	0.73
250	2	18	43	0.41
500	2	22	37	0.43
$\Omega = 100$ $Pe_{particle}$	$\{ReSc\}_{critical} = 176$ φ correlation	Pe_{MT}	Maximum Conversion (%)	α
1	1	10	99	0.33
10	1	18	95	0.48
50	1	24	87	0.79
100	1	27	82	0.99
250	2	28	83	0.84
500	2	48	65	0.46

densities in the bulk fluid phase, because $\alpha > 0$. Maximum conversion increases at larger chemical reaction coefficients and smaller particle-based mass transfer Peclet numbers (ie, the ratio of Ω to $Pe_{particle}$ scales as the square of residence time). The corresponding value of Pe_{MT}, which yields maximum conversion, increases at larger chemical reaction coefficients and larger $Pe_{particle}$.

These trends are illustrated in Figures 1–3. When the chemical reaction coefficient remains constant, the presence of both interpellet axial dispersion and external mass transfer resistance in tubular reactor simulations reveals that higher conversion of reactants to products is achieved at shorter residence times, over a restricted range of subcritical mass transfer Peclet numbers. These nontraditional results are attributed to the analysis of external mass transfer resistance in isothermal packed catalytic tubular reactors.

2.12. Examples of Packed Catalytic Tubular Reactor Design with External Mass Transfer Resistance. A packed catalytic tubular reactor (radius R_{PFR} and length L_{PFR}) contains porous spherical catalysts (radius R_{sphere}) and operates at the following values of the important dimensionless numbers that govern reactor performance. The reaction kinetics are second-order irreversible (ie, $n = 2$) and the rate law depends only on the molar density of reactant A on the external surface of the catalyst [ie, $k_2(C_{A,Surface})^2$].

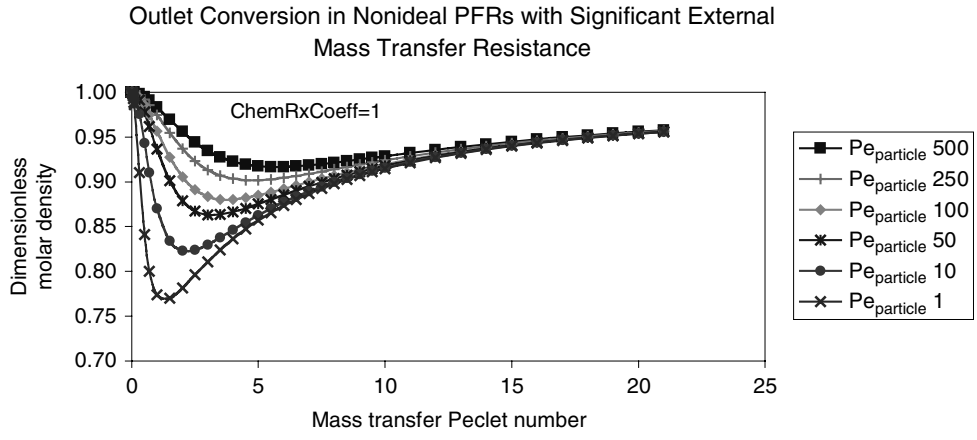

Fig. 1. Effect of the mass transfer Peclet number Pe_{MT} and Pe_{particle} ($= Pe_{\text{Simple}}$) on dimensionless reactant molar density in the exit stream (ie, $\zeta_{\text{PFR}} = 1$) of nonideal packed catalytic tubular reactors with first-order irreversible chemical kinetics, external mass transfer resistance, $\varepsilon_{p,\text{interpellet}} = 0.50$, and $\Omega = \text{ChemRxCoeff} = 1$.

Intrapellet Damköhler number (characteristic length is R_{sphere}), $\Lambda^2_{A,\text{intrapellet}} = 4$.

Interpellet Damköhler number, $\Lambda^2_{A,\text{interpellet}} = 14$.

Mass transfer Peclet number, $Pe_{MT} = 3$.

Particle-based mass transfer Peclet number, $Pe_{\text{particle}} = 50$.

Interpellet porosity, $\varepsilon_{p,\text{interpellet}} = 0.5$.

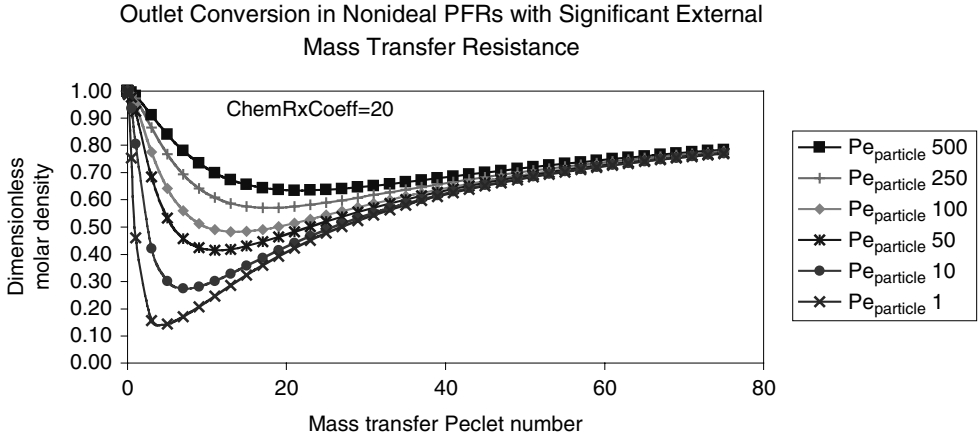

Fig. 2. Effect of the mass transfer Peclet number Pe_{MT} and Pe_{particle} ($= Pe_{\text{Simple}}$) on dimensionless reactant molar density in the exit stream (ie, $\zeta_{\text{PFR}} = 1$) of nonideal packed catalytic tubular reactors with first-order irreversible chemical kinetics, external mass transfer resistance, $\varepsilon_{p,\text{interpellet}} = 0.50$, and $\Omega = \text{ChemRxCoeff} = 20$.

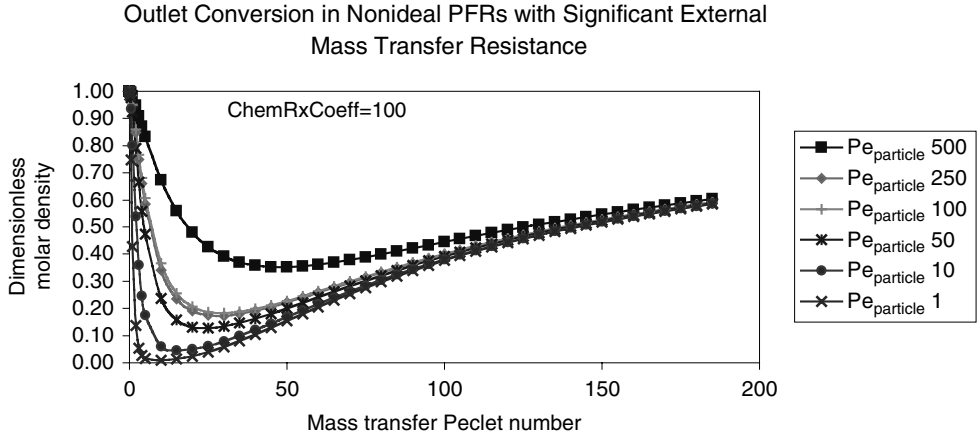

Fig. 3. Effect of the mass transfer Peclet number Pe_{MT} and Pe_{particle} ($= Pe_{\text{Simple}}$) on dimensionless reactant molar density in the exit stream (ie, $\zeta_{\text{PFR}} = 1$) of nonideal packed catalytic tubular reactors with first-order irreversible chemical kinetics, external mass transfer resistance, $\varepsilon_{p,\text{interpellet}} = 0.50$, and $\Omega = \text{ChemRxCoeff} = 100$.

Nonideal Design. The initial step in the overall design strategy is to consult Table 18-1 in *Transport Phenomena for Chemical Reactor Design*, by Belfiore (2), where pseudo-homogeneous radial diffusion and pseudo-volumetric second-order irreversible chemical reaction in spherical catalysts are characterized numerically by an effectiveness factor $E = 0.71$ when the intrapellet Damköhler number (ie, $\Lambda^2_{A,\text{intrapellet}}$) is 4. The chemical reaction coefficient is approximately 5 (actually 4.97). Hence, Table 1 reveals that the mass transfer Peclet number Pe_{MT} is 10-fold smaller than $\{\text{Re}Sc\}_{\text{critical}}$, and Table 2 indicates that external mass transfer resistance is significant, because $\alpha \approx 2.5$. Based on the definition of dimensionless reactant molar density via equation 23, final conversion in this nonideal tubular reactor is given by $\xi_{\text{final}} = 1 - \Psi_{A,\text{BulkGas,Real}}(\zeta_{\text{PFR}} = 1) = 20\%$ (ie, 0.20).

Effect of Reactor Length. If the reactor length is tripled (ie, three-fold increase in L_{PFR}) while maintaining the same pellet packing density, then the particle-based dimensionless numbers are not affected. Hence, the intrapellet Damköhler number, the effectiveness factor, and the particle-based mass transfer Peclet number do not change. The interpellet porosity of the packed bed remains constant, according to the design statement. The mass transfer Peclet number scales as L_{PFR}, and the interpellet Damköhler number scales as the square of L_{PFR} (ie, see eqs. 25 and 26). If reactor length increases by a factor of 3, then $Pe_{MT} = 9$ (ie, increases by a factor of 3) and $\Lambda^2_{A,\text{interpellet}} = 126$ (ie, increases by a factor of 9). There is no change in α, which remains constant at a numerical value of 2.5 as the reactor length increases by a factor of 3. In general, α is independent of reactor length. Alpha scales as the ratio of the interpellet Damköhler number to the square of the mass transfer Peclet number, both of which scale as L^2_{PFR}, yielding no dependence of α on L_{PFR} via equation 57. No other dimensionless numbers in the definition of α depend on L_{PFR}. If the kinetics were first-order irreversible, instead of second-order, then one predicts 77% final conversion in ideal packed catalytic tubular reactors via equation 46 when

external mass transfer resistance cannot be neglected and L_{PFR} is 3-fold larger. Alpha remains constant at 2.85 for first-order kinetics as L_{PFR} increases by a factor of 3. The only difference between $\alpha = 2.5$ for second-order kinetics and $\alpha = 2.85$ for first-order kinetics is due to the effectiveness factor in spherical catalytic pellets ($E = 0.71$ for $n = 2$ vs. $E = 0.81$ for $n = 1$ when $\Lambda^2_{A,\text{intrapellet}} = 4$). The classic isothermal dimensionless correlation that summarizes intrapellet radial diffusion and first-order irreversible chemical reaction in spheres is (2,13).

$$E = \frac{3}{\Lambda^2_{A,\text{intrapellet}}} \left\{ \frac{\Lambda_{A,\text{intrapellet}}}{\tanh \Lambda_{A,\text{intrapellet}}} - 1 \right\} \tag{58}$$

Effect of Volumetric Flowrate. If the volumetric flowrate is tripled (ie, three-fold increase in q) while maintaining the same pellet packing density, then the intrapellet Damköhler number and the effectiveness factor are not affected. The particle-based mass transfer Peclet number increases by a factor of 3 because it is defined via equation 55 in terms of the average interstitial fluid velocity between the catalytic pellets. As Pe_{particle} increases from 50 to 150, the correlation coefficient for interpellet axial dispersion increases from 1 to 2. Hence, the mass transfer Peclet number decreases by a factor of 2, from 3 to 1.5 via equation 56, because the interpellet axial dispersion coefficient appears in the denominator of Pe_{MT}. There is no other effect of flowrate on Pe_{MT}. As interpellet axial dispersion coefficients increase by a factor of 6 (ie, 3-fold increase in the interstitial fluid velocity and a 2-fold increase in the correlation coefficient from the dimensional analysis of *flow through porous media*), the interpellet Damköhler number decreases from 14 to 2.33 when the volumetric flowrate triples. Alpha decreases because there is less mass transfer resistance in the gas-phase boundary layer external to the catalytic pellets, producing an increase in mass transfer coefficients at higher flowrates. In the creeping flow regime, mass transfer coefficients in the gas-phase boundary layer scale as the one-third power of the particle-based Reynolds number via equation 53, which includes the interstitial fluid velocity. Interpellet axial dispersion coefficients scale linearly with q via their dependence on the interstitial fluid velocity between the catalytic pellets, and interpellet Damköhler numbers scale inversely with q. As flowrate affects the chemical reaction coefficient Ω and Pe_{particle}, equation 57 reveals that α scales as $q^{-1/3}$ for creeping flow. The correlation coefficient for interpellet axial dispersion does not affect α. Hence, if q increases 3-fold, then α decreases by 1.4, or $3^{1/3}$. If the kinetics were first-order irreversible, instead of second-order, then one predicts 19% final conversion in ideal packed catalytic tubular reactors via equation 46 when external mass transfer resistance cannot be neglected. Reactant conversion is governed primarily by a 3-fold decrease in residence time. Alpha actually decreases from 2.85 to 2.0 when the kinetics are first-order irreversible and the volumetric flowrate triples. This agrees with $\alpha \approx q^{-1/3}$.

Effect of Particle Size. If the diameter of the spherical catalytic pellets is reduced by a factor of 2 (ie, 2-fold decrease in R_{sphere}) while maintaining the same pellet packing density, then both the particle-based and vessel-based dimensionless numbers are affected. As the intrapellet Damköhler number scales as the square of the pellet radius (ie, see equation 76), a 2-fold decrease in R_{pellet}

produces a 4-fold decrease in $\Lambda^2_{A,\text{intrapellet}}$ from 4 to 1, and a corresponding increase in the effectiveness factor from 0.71 to 0.89 as summarized in Table 18-1 of *Transport Phenomena for Chemical Reactor Design*, by Belfiore (2), for second-order irreversible chemical reaction in spheres. As the particle diameter for spherical catalysts represents the characteristic length in Pe_{particle}, the particle-based mass transfer Peclet number decreases 2-fold from 50 to 25, and the correlation coefficient for interpellet axial dispersion remains constant at $\varphi_{\text{correlation}} = 1$. The mass transfer Peclet number scales inversely with particle size via equation 56, so Pe_{MT} increases 2-fold from 3 to 6. Interpellet axial dispersion coefficients scale linearly with particle size, so a 2-fold decrease in pellet diameter produces a 2-fold decrease in interpellet axial dispersion coefficients and a corresponding 2-fold increase in the interpellet Damköhler number from 14 to 28. The effect of particle size, or the equivalent diameter of a single catalytic pellet $d_{\text{equivalent}}$, on α depends on the magnitude of the intrapellet Damköhler number because the effectiveness factor scales inversely with $d_{\text{equivalent}}$ only in the diffusion-limited regime (ie, $E \approx 1/\Lambda_{A,\text{intrapellet}}$) at large values of $\Lambda_{A,\text{intrapellet}}$. In general, interpellet axial dispersion coefficients scale linearly with $d_{\text{equivalent}}$ and the mass transfer Peclet number scales inversely with $d_{\text{equivalent}}$. Hence, in the diffusion-limited regime, the chemical reaction coefficient scales inversely with $d^2_{\text{equivalent}}$ via the effectiveness factor and the interpellet Damköhler number. Now, the effects of $d_{\text{equivalent}}$ on α via the chemical reaction coefficient and the mass transfer Peclet number cancel, so the only remaining dependence of α on $d_{\text{equivalent}}$ is due to the particle-based mass transfer Peclet number, so $\alpha \approx (d_{\text{equivalent}})^{2/3}$ because Pe_{particle} scales linearly with $d_{\text{equivalent}}$. When particle size decreases by a factor of 2, the previous scaling law in the diffusion-limited regime suggests that α decreases by 1.6, or $2^{2/3}$. If one neglects the effect of particle size on the effectiveness factor in the extreme reaction-rate-controlled regime at very small values of the intrapellet Damköhler number (ie, $E \approx 1$, isothermally), then the chemical reaction coefficient scales inversely with $d_{\text{equivalent}}$ via the interpellet Damköhler number, the ratio of the chemical reaction coefficient to Pe^2_{MT} scales linearly with $d_{\text{equivalent}}$, and $\alpha \approx (d_{\text{equivalent}})^{5/3}$. When particle size decreases 2-fold, this scaling law suggests that α decreases by 3.2, or $2^{5/3}$. Actual calculations for first-order irreversible chemical reaction indicate that α decreases by a factor of 2.85, from 2.85 to 1.0, when the diameter of these spherical catalytic pellets decreases 2-fold, the intrapellet Damköhler number $\Lambda^2_{A,\text{intrapellet}}$ decreases 4-fold, and the effectiveness factor increases from $E = 0.81$ when $\Lambda^2_{A,\text{intrapellet}} = 4$ to $E = 0.94$ when $\Lambda^2_{A,\text{intrapellet}} = 1$. The actual scaling law is somewhere between $\alpha \approx (d_{\text{equivalent}})^{5/3}$ at small intrapellet Damköhler numbers, and $\alpha \approx (d_{\text{equivalent}})^{2/3}$ at large intrapellet Damköhler numbers, which is consistent with the fact that $\Lambda^2_{A,\text{intrapellet}} = 1$. One predicts 66% conversion of reactants to products in ideal packed catalytic tubular reactors with first-order irreversible chemical kinetics via equation 46 when external mass transfer resistance cannot be neglected and particle size decreases by a factor of 2.

Effect of Reactor Diameter. If the tubular reactor diameter is doubled (ie, 2-fold increase in R_{PFR}) while maintaining the same pellet packing density, then the intrapellet Damköhler number and the effectiveness factor are not affected. The particle-based mass transfer Peclet number decreases 4-fold, from 50 to 12.5, because the average interstitial fluid velocity is 4-fold smaller if the volumetric flowrate remains constant and the flow cross-sectional area

experiences a 4-fold increase. In this range of Pe_{particle}, the correlation coefficient that relates interpellet axial dispersion to Pe_{particle} does not change, and neither does the mass transfer Peclet number Pe_{MT}. As the average interstitial fluid velocity experiences a 4-fold decrease, so does the interpellet axial dispersion coefficient, which causes the interpellet Damköhler number to increase by a factor of four, from 14 to 56, when the reactor diameter is doubled. The primary reason that α increases is because the average interstitial velocity decreases when the flow cross-sectional area increases and the volumetric flowrate remains constant. A few important dimensionless numbers are affected by $\langle v_z \rangle_{\text{interstitial}}$. The interpellet Damköhler number and the chemical reaction coefficient increase by a factor of four, whereas the particle-based mass transfer Peclet number decreases by a factor of four. Mass transfer resistance increases in the external gas-phase boundary layer when the interstitial fluid velocity decreases. In the creeping flow regime, mass transfer coefficients scale as the one-third power of the particle-based Reynolds number, which includes the interstitial fluid velocity. This effect is accounted for by the dependence of the particle-based surface-averaged Sherwood number on Pe_{particle} for creeping flow around submerged objects. Equation 57 reveals that α scales as $(R_{\text{PFR}})^{2/3}$ for creeping flow, via consideration of the effect of R_{PFR} on the chemical reaction coefficient Ω, or the interpellet Damköhler number, and Pe_{particle}. Hence, if R_{PFR} increases 2-fold, then α increases by 1.6, or $2^{2/3}$. If the kinetics were first-order irreversible, not second-order, then one predicts 75% final conversion in ideal packed catalytic tubular reactors via equation 46, primarily because residence time τ increases by a factor of four with significant external mass transfer resistance. One of the previous examples reveals that ideal packed catalytic tubular reactors achieve 77% conversion when L_{PFR} triples, which corresponds to a 3-fold increase in residence time with $\alpha = 2.85$ and first-order irreversible kinetics. When the reactor radius increases 2-fold and residence time increases 4-fold, one achieves slightly less conversion (ie, 75%), relative to the 3-fold increase in τ that corresponds to a 3-fold increase in L_{PFR}, because α increases from 2.85 to 4.5 when R_{PFR} is doubled. This agrees with $\alpha \approx (R_{\text{PFR}})^{2/3}$ and illustrates the combined effects of residence time and external mass transfer resistance on final conversion in ideal packed catalytic tubular reactors. Equation 57 illustrates the dependence of α on some important dimensionless parameters that govern the performance of packed catalytic tubular reactors. This correlation is exact in the creeping flow regime. The four numerical examples discussed in this article reveal an equivalent creeping-flow scaling law for α in terms of some important dimensional parameters.

$$\alpha \approx \frac{R_{\text{PFR}}^{2/3} d_{\text{equivalent}}^{\gamma}}{q^{1/3}} \neq f(L_{\text{PFR}}) \qquad \frac{2}{3} \leq \gamma < \frac{5}{3} \tag{59}$$

where the exponent γ is a decreasing function of the intrapellet Damköhler number. For example, γ is slightly less than 5/3 when $\Lambda_{A,\text{intrapellet}}$ approaches zero in the extreme reaction-rate-controlled regime, and $\gamma = 2/3$ at very large values of the intrapellet Damköhler number in the diffusion-controlled regime where the effectiveness factor scales inversely with $\Lambda_{A,\text{intrapellet}}$.

2.13. Maximum Temperature in Macroporous Catalysts with Exothermic Chemical Reaction in the Diffusion-Controlled Regime. The classic Prater equation (6,15–17) relates temperature and reactant molar density in porous catalysts when (*1*) only one chemical reaction occurs, (*2*) all physicochemical properties of the reactive mixture exhibit no temperature dependence, and (*3*) thermal diffusion is not considered. When catalysts operate in the diffusion-controlled regime at large intrapellet Damköhler numbers (18), the Prater equation suggests that there is a simple linear relation between maximum intrapellet temperatures near the central core of the catalyst and the Prater number β, where β is defined in equation 64. This relation between maximum intrapellet temperature and the Prater number exhibits significant deviations from linearity when the analysis of coupled heat and mass transfer in macroporous catalysts includes thermal diffusion and temperature-dependent physicochemical properties of the reactive gas mixture. Numerical analysis is required, in general, to obtain the desired nonlinear relation between maximum intrapellet temperature and the Prater number β, which reveals that β has a practical upper limit for steady-state simulations to prevent core temperatures from increasing by a few orders of magnitude relative to conditions on the external catalytic surface. This restriction on the magnitude of the Prater number for exothermic chemical reactions is not obvious from the original Prater equation, and there are very few publications in the Web of Science database that focus on maximum temperature in porous catalysts with exothermic chemical reaction. There seems to be a dearth of publications that address intrapellet coupled heat and mass transfer with exothermic chemical reaction in the presence of thermal diffusion (ie, the Soret effect). The following subsections of this article consider steady-state analysis of the microscopic mass transfer equation and the thermal energy balance with one chemical reaction in porous catalysts. Convective transport in neglected. Equation 60 is valid in the presence or absence of thermal diffusion, whereas thermal diffusion is neglected in equations 61 and 62. These equations and their dimensionless analogs provide the starting point for numerical analysis of maximum intrapellet temperature in the diffusion-controlled regime where the central core of the catalyst is starved of reactants.

Theoretical Considerations. Steady-state analysis of coupled heat and mass transfer in porous catalysts, with negligible convective transport, allows one to relate temperature and species molar density profiles in isolated pellets. The intrapellet thermal energy balance based on equations 9–13 is revisited, including the stoichiometric relation among intrapellet diffusional fluxes (ie, equation 4), to estimate the temperature increase due to exothermic reaction. For example, if $\underline{\mathbf{n}}$ is a unit normal vector directed from the pellet into the bulk gas stream, and the molecular flux of thermal energy contains contributions from thermal conduction (ie, Fourier's law) and the interdiffusional flux via the coupling between heat and mass transfer, then equation 60 is valid everywhere within the pellet;

$$\underline{n}\cdot\underline{q}=\underline{n}\cdot\left\{-k_{\text{effective}}\nabla T_{\text{pellet}}+\sum_{i=1}^{N}\frac{\bar{H}_i}{MW_i}j_{i,\text{pellet}}\right\}=0$$

$$\underline{n}\cdot\{k_{\text{effective}}\nabla T_{\text{pellet}}\}=\sum_{i=1}^{N}\frac{\bar{H}_i}{MW_i}\{\underline{n}\cdot j_{i,\text{pellet}}\}=\frac{1}{\upsilon_A MW_A}\{\underline{n}\cdot j_{A,\text{pellet}}\}\sum_{i=1}^{N}\upsilon_i\bar{H}_i \qquad (60)$$

$$\underset{\upsilon_A=-1}{\Rightarrow}\frac{1}{MW_A}\{\underline{n}\cdot j_{A,\text{pellet}}\}(-\Delta H_{\text{Reaction}})$$

The diffusional molar flux of reactant A in the direction of $\underline{\mathbf{n}}$ is expressed in terms of a molar density gradient within the pellet and an effective intrapellet diffusivity, $D_{A,\text{effective}}$, via equation 66, (ie, thermal diffusion is considered later in this article). Hence,

$$\frac{1}{MW_A}\{\underline{n}\cdot j_{A,\text{pellet}}\} = -D_{A,\text{effective}}\frac{\partial C_{A,\text{pellet}}}{\partial n} \tag{61}$$

where n is a spatial coordinate that increases in the direction of $\underline{\mathbf{n}}$, and the temperature dependence of $D_{A,\text{effective}}$ is governed by pore size. Intrapellet conductive and diffusional fluxes in equation 60 are evaluated in the normal coordinate direction, relative to the external surface of the catalyst. The desired relation between temperature and reactant molar density is applicable to multi-dimensional transport in porous catalysts of any geometry, but the stoichiometric condition among diffusional mass fluxes given by equation 4 limits this analysis to one chemical reaction (2). As illustrated by equation 62, which is applicable everywhere throughout an isolated pellet, spatial coordinate n does not appear in the final result

$$\begin{aligned}\underline{n}\cdot\{k_{\text{effective}}\nabla T_{\text{pellet}}\} = k_{\text{effective}}\frac{\partial T_{\text{pellet}}}{\partial n} &= -(-\Delta H_{\text{Reaction}})D_{A,\text{effective}}\frac{\partial C_{A,\text{pellet}}}{\partial n}\\ \frac{\partial T_{\text{pellet}}}{\partial C_{A,\text{pellet}}} &= \frac{-(-\Delta H_{\text{Reaction}})D_{A,\text{effective}}}{k_{\text{effective}}}\end{aligned} \tag{62}$$

Dimensional Analysis of Intrapellet Temperature. For isolated pellets, dimensionless variables (ie, Θ and $\Psi_{A,\text{pellet}}$) are introduced using the characteristic temperature T_{Surface} and reactant molar density $C_{A,\text{Surface}}$ on the external surface of the catalyst. Hence,

$$\Theta = \frac{T_{\text{pellet}}}{T_{\text{Surface}}};\ \Psi_{A,\text{pellet}} = \frac{C_{A,\text{pellet}}}{C_{A,\text{Surface}}} \tag{63}$$

The thermal energy generation parameter β, also known as the Prater number (2,6,15–17), strongly influences temperature profiles within the catalyst. If one accounts for the temperature dependence of effective intrapellet diffusivities and the enthalpy change for chemical reaction (ie, see eq. 15), then dimensional analysis of equation 62 yields

$$\begin{aligned}\frac{\partial\Theta}{\partial\Psi_{A,\text{pellet}}} &= \frac{-D_{A,\text{effective}}(T_{\text{Surface}})C_{A,\text{Surface}}\{-\Delta H_{\text{Reaction}}(T_{\text{Surface}})\}}{T_{\text{Surface}}k_{\text{effective}}}\\ &\quad\left[\frac{D_{A,\text{effective}}(T_{\text{pellet}})}{D_{A,\text{effective}}(T_{\text{Surface}})}\right]\left\{\frac{\Delta H_{\text{Reaction}}(T_{\text{pellet}})}{\Delta H_{\text{Reaction}}(T_{\text{Surface}})}\right\}\\ &= -\beta\varepsilon(\Theta)\zeta(\Theta)\\ \beta &= \frac{D_{A,\text{effective}}(T_{\text{Surface}})C_{A,\text{Surface}}\{-\Delta H_{\text{Reaction}}(T_{\text{Surface}})\}}{T_{\text{Surface}}k_{\text{effective}}} = \text{Prater \#}\end{aligned} \tag{64}$$

The Prater number β, which is positive for exothermic reactions (6,15–17), should be calculated using conditions on the external catalytic surface (2). $\varepsilon(\Theta)$ represents a ratio of effective intrapellet diffusivities at temperature T_{pellet} relative to temperature on the external surface of the catalyst, and $\zeta(\Theta)$ is the ratio of the enthalpy change for chemical reaction at intrapellet temperature T_{pellet} relative to $\Delta H_{\text{Reaction}}$ at the external catalytic surface temperature. The product of the Prater number and the intrapellet Damköhler number (ie, $\beta\Lambda^2_{A,\text{intrapellet}}$, where the intrapellet Damköhler number is defined by equation 76) essentially represents a ratio of the rate of thermal energy generation due to chemical reaction relative to the rate of thermal conduction (ie, via Fourier's law) within the catalyst. In the diffusion-limited regime at large values of the intrapellet Damköhler number (18), the central core of the catalyst is reactant-starved (ie, $\Psi_{A,\text{pellet}} \Rightarrow 0$ as the dimensionless spatial coordinate $\eta \Rightarrow 0$) and significant temperature increases occur within the catalyst when the reaction is exothermic. Under these conditions, the Prater equation (2,6,15–17) provides a *zeroth-order* prediction for the maximum dimensionless temperature, $\Theta_{\max} \approx 1 + \beta$, near the center of the catalyst when the temperature dependence of (*1*) effective intrapellet diffusivities and (*2*) the enthalpy change for chemical reaction are neglected [ie, $\varepsilon(\Theta) \approx 1$, $\zeta(\Theta) \approx 1$]. When simple temperature dependence of intrapellet diffusion coefficients is considered [ie, $\varepsilon(\Theta) \approx \Theta^m$, with $m = 0.5$ for nanopores and $m = 1.5$ for macropores; $\zeta(\Theta) \approx 1$], a better prediction for the maximum dimensionless temperature is obtained via integration of equation 64 for Θ vs. $\Psi_{A,\text{pellet}}$, when $\Psi_{A,\text{pellet}} \Rightarrow 0$ as $\eta \Rightarrow 0$ for diffusion-controlled operation (2). Hence,

$$\frac{\partial\Theta}{\partial\Psi_{A,\text{pellet}}} = -\beta\varepsilon(\Theta) \approx -\beta\Theta^m$$
$$\Theta_{\max}^{1-m} \approx 1 + (1-m)\beta\{1 - \Psi_{A,\text{pellet}}(\eta = 0)\} \Rightarrow 1 + (1-m)\beta \tag{65}$$

Now, the upper limit for the thermal energy generation parameter is $\beta < 2$ in the macropore regime, because steady-state predictions of $\Theta_{\max}$ tend toward infinity when $\varepsilon(\Theta) \approx \Theta^{1.5}$, $m = 3/2$, and $\beta = 2$.

2.14. Effect of the Diffusion Collision Integral on Maximum Intrapellet Temperature in Macroporous Catalysts. The kinetic theory of dilute gases (19–21) describes the complete temperature dependence of ordinary molecular diffusion coefficients.

$$D_{A,\text{ordinary}} \approx \frac{T^{3/2}}{p\sigma^2\Omega_D(T)}$$
$$D_{A,\text{effective}} = \frac{\varepsilon_{p,\text{intrapellet}}}{\tau_{or}} D_{A,\text{ordinary}} \tag{66}$$

The internal structure of the catalytic pores is described by an intrapellet void volume fraction $\varepsilon_{p,\text{intrapellet}}$ and tortuosity factor τ_{or}, where the former represents an average over pore size and the latter averages the orientation of *parallel pores* (2,6). Equation 66 contains the dominant resistance to intrapellet mass transfer in macroporous catalysts where the average pore size is typically greater than 1 μm. The collision integral Ω_D, which quantitatively summarizes

the dynamics of molecular trajectories and binary collisions for dilute gas mixtures (19), provides a correction to the *hard sphere intermolecular potential energy* because realistic molecules do not collide like hard spheres when the repulsive part of the potential exhibits some degree of *softness*. As diffusion is inherently a "mixture property," collision cross-sections and collision integrals for diffusion, which scale as $1-\cos\chi$ where χ is the deflection angle in a collision, are slightly smaller than those for viscosity and thermal conductivity of pure materials, which scale as $1-\cos^2\chi$, at least as a first-order approximation for these isotropic transport properties (19–21). Relative to rigid spheres with collision diameter σ for low-energy collisions, *Lennard–Jones molecules* have a slightly smaller cross-section for high-energy collisions that are almost *head-on*, due to strong repulsive forces. The influence of attractive forces when intermolecular separations are greater than their equilibrium values is responsible for the fact that collision cross-sections for diffusion can be almost 6-fold larger than the corresponding rigid-sphere cross-sections for low-energy "grazing" collisions (19). Numerical simulations in this article include temperature dependence of the collision integral Ω_D for diffusion in $\varepsilon(\Theta)$, as proposed by Neufeld et al. (22) for molecules that follow the Lennard–Jones 6-12 potential energy of interaction

$$\begin{aligned}\Omega_D(T^*) &\approx A\{T^*\}^{-B} + C\exp\{-DT^*\} + E\exp\{-FT^*\} + G\exp\{-HT^*\}\\ T^* &= \frac{k_{\text{Boltzmann}}T_{\text{Surface}}\Theta}{\varepsilon_{\text{Lennard-Jones}}};\quad A = 1.06036;\quad B = 0.15610;\quad C = 0.19300\\ D &= 0.47635;\quad E = 1.03587;\quad F = 1.52996;\quad G = 1.76474;\quad H = 3.89411\end{aligned} \tag{67}$$

in addition to the three-halves power of dimensionless temperature for large pores. There are no distinguishable differences between the previous empirical equation and tabulated values of the diffusion collision integral from *Transport Phenomena*, by Bird et al. (13), for dimensionless temperatures T^* between 0.30 and 100. As a consequence of including Ω_D in the ratio of effective intrapellet diffusivities in equation 64, there is an additional dimensionless parameter that affects the maximum temperature rise in adiabatic pellets with exothermic chemical reaction (ie, $k_{\text{Boltzmann}}T_{\text{Surface}}/\varepsilon_{\text{Lennard-Jones}}$). The maximum depth of the Lennard–Jones potential energy function, or the maximum energy of attraction when molecules reside at their equilibrium separation distance [ie, $\sigma(2)^{1/6}$], is given by $\varepsilon_{\text{Lennard-Jones}}/k_{\text{Boltzmann}}$ with dimensions of absolute temperature, where $k_{\text{Boltzmann}}$ is Boltzmann's constant. Now, one must integrate the following equation, with $\zeta(\Theta) \approx 1$:

$$\frac{\partial\Theta}{\partial\Psi_{A,\text{pellet}}} = -\beta\varepsilon(\Theta) \approx -\beta\Theta^{1.5}\left\{\frac{\Omega_D(\Theta=1)}{\Omega_D(\Theta)}\right\} \tag{68}$$

numerically from the external surface, where dimensionless temperature Θ and molar density $\Psi_{A,\text{pellet}}$ are unity, *inward* toward the center of the catalyst where the molar density of reactant A tends toward zero in the diffusion-controlled regime at large values of the intrapellet Damköhler number. It is necessary to transform the independent variable from dimensionless molar density $\Psi_{A,\text{pellet}}$ to $1-\Psi_{A,\text{pellet}}$, so that the new independent variable begins at zero on the

external surface and achieves a value of 1 at the center of the pellet, as required by numerical ODE solvers. Unlike isothermal problems with diffusion and chemical reaction, equation 68 exhibits no singularity at the center of catalysts with cylindrical or spherical symmetry (2). As a consequence of this change in independent variable from $\Psi_{A,\text{pellet}}$ to $1-\Psi_{A,\text{pellet}}$, it is necessary to remove the negative sign in equation 68. A second-order predictor-corrector algorithm was implemented with automatic step-size adjustment that is useful for integrating stiff differential equations. As a general rule, the effect of the collision integral for diffusion and its temperature dependence on the maximum temperature near the center of the catalyst is insignificant for thermal energy generation parameters (ie, Prater numbers) $\beta < 0.5$. Under mild intrapellet conditions (ie, $\beta < 0.5$), $\Theta_{\max} \approx \{1 - \beta/2\}^{-2}$ provides reasonably accurate estimates of the temperature increase due to exothermic chemical reaction in macroporous catalysts (2). This claim is based on comparisons of $\Theta_{\max}$, with and without the ratio of collision integrals in equation 68 at various Prater numbers. Froment and Bischoff (6) calculate typical Prater numbers for ten exothermic catalytic reactions, and only the dissociation of N_2O is characterized by $\beta > 0.5$ (actually $\beta = 0.64$). For example, macroporous alumina catalysts with effective thermal conductivities of 1.6×10^{-3} J/cm-s-K, surface temperatures near 350K, and reactant molar densities estimated via the ideal gas law at T_{Surface} and ambient pressure require enthalpy changes for chemical reaction on the order of 120 kJ/mol (ie, $\approx$29 kcal/mol) to achieve a Prater number of unity (2). Hence, intrapellet temperatures are not predicted to increase significantly in many cases because large effective thermal conductivities (ie, $k_{\text{effective}}$) of metallic or metal-coated ceramic porous catalysts produce efficient intrapellet heat transfer. This is one primary reason why typical Prater numbers do not exceed unity. However, the strongly exothermic hydrogenation of benzene to cyclohexane over a supported-nickel catalyst (1,23) is described by Prater numbers that approach 0.95 (ie, $\Delta H_{\text{Reaction}} \approx 50$ kcal/mol). When temperature dependence of the collision integral Ω_D for diffusion is considered, numerical simulations reveal that it is difficult to predict steady-state temperature profiles in macroporous catalysts with exothermic chemical reaction when the thermal energy generation parameter β achieves values between 1.25 and 1.35. This upper limit of β for realistic predictions depends on the ratio of the catalytic surface temperature T_{Surface} to the Lennard–Jones characteristic temperature (ie, $T_{\text{Lennard–Jones}}$), where the latter is defined by the ratio of the maximum potential well depth $\varepsilon_{\text{Lennard–Jones}}$ to Boltzmann's constant $k_{\text{Boltzmann}}$. The upper limit of β is larger (ie, $\beta \Rightarrow 1.35$) for reasonable predictions of $\Theta_{\max}$ when $T_{\text{Surface}}/T_{\text{Lennard–Jones}}$ increases. Obviously, $\Theta_{\max}$ increases when β is larger and $T_{\text{Surface}}/T_{\text{Lennard–Jones}}$ remains constant. However, $\Theta_{\max}$ decreases when $T_{\text{Surface}}/T_{\text{Lennard–Jones}}$ is larger at a constant Prater number. These trends are illustrated in Figure 4 for intrapellet diffusion of carbon monoxide (ie,$T_{\text{Lennard–Jones}} = 110$K) (19) when the external catalytic surface temperature, T_{Surface}, is either 300K, 400K, or 900K.

2.15. Effect of Temperature-Dependent Enthalpy Changes for Exothermic Chemical Reaction on the Maximum Temperature in Macroporous Catalysts. *Production of Methanol from a Moderately High-Pressure Stoichiometric Feed of Carbon Monoxide and Hydrogen.* This specific example illustrates how the maximum intrapellet temperature for exothermic reactions is

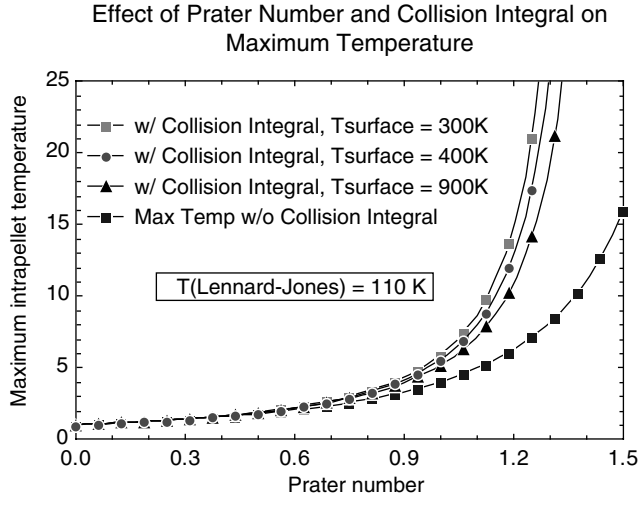

Fig. 4. Effect of the Prater number and the collision integral for ordinary molecular diffusion on the maximum dimensionless intrapellet temperature of macroporous catalysts in the diffusion-controlled regime at large values of the intrapellet Damköhler number. Calculations are presented for carbon monoxide, whose maximum intermolecular energy of attraction is described by a Lennard–Jones temperature (or potential well depth, divided by Boltzmann's constant) of 110K. The Lennard–Jones temperature and the temperature on the external catalytic surface represent additional parameters that appear in the collision integral. For Prater numbers β greater than 1, there are significant differences between the maximum intrapellet temperature when the collision integral is included in the analysis, relative to the lowest curve that excludes the collision integral. Maximum temperature predictions without the collision integral correspond to $\Theta_{max} \approx \{1-\beta/2\}^{-2}$. Predictions from the original Prater equation yield $\Theta_{max} \approx 1+\beta$.

affected by including temperature dependence in $\Delta H_{Reaction}$ via equation 15, such that $\zeta(\Theta) \neq 1$ in equations 64 and 68. The synthesis of methanol from C≡O and H_2 in gas-phase packed catalytic tubular reactors is industrially important. Consequently, a large amount of experimental data is available to characterize this reaction over a wide range of operating pressures (24–28). As there are no H–H bonds in the final product, a 5-site chemical reaction between adsorbed species on zinc chromite catalysts (ie, ZnO/Cr_2O_3) (2,24,25) is considered to be the rate-limiting step for $CO + 2H_2 \Leftrightarrow CH_3OH$, with nonpreferential dissociative adsorption of atomic hydrogen (ie, H) on adjacent active sites. The synthesis of methanol over Cu-based catalysts (26) seems to occur exclusively by CO_2 hydrogenation at lower operating pressures. Equations 64, 66, 67, and 68 with $\zeta(\Theta) \neq 1$ provide the starting point for analysis of coupled heat and mass transfer in macroporous catalysts with temperature-dependent physicochemical properties, like $D_{A,effective(T_{pellet})}$ contained in $\varepsilon(\Theta)$ and $\Delta H_{Reaction}(T_{pellet})$ in $\zeta(\Theta)$.

$$\frac{\partial \Theta}{\partial \Psi_{A,pellet}} = -\beta\varepsilon(\Theta)\zeta(\Theta)$$

$$\zeta(\Theta) \approx \frac{\Delta H^0_{\text{Reaction,298K}} + \sum_{i=1}^{N} \upsilon_i \int_{298\text{K}}^{T=\Theta T_{\text{Surface}}} C_{p,i}(T')dT'}{\Delta H^0_{\text{Reaction,298K}} + \sum_{i=1}^{N} \upsilon_i \int_{298\text{K}}^{T_{\text{Surface}}} C_{p,i}(T')dT'} \qquad (69)$$

$$C_{p,i}(T) \approx a_i + b_i T + c_i T^2 + d_i T^3$$

The standard state enthalpy change at 298K, $\Delta H^0{}_{\text{Reaction,298K}}$, for the synthesis of methanol from carbon monoxide and hydrogen is −21.7 kcal/mol. The maximum energy of attraction for this Lennard–Jones ternary gas mixture, $\varepsilon_{\text{ABC}}/k_{\text{Boltzmann}}$, is estimated from a geometric average of pure-component potential well depths (2,13,19) when molecules reside at their equilibrium separation distances.

$$\frac{\varepsilon_{\text{ABC}}}{k_{\text{Boltzmann}}} \approx \frac{\sqrt[3]{\varepsilon_{\text{C}\equiv\text{O}}\varepsilon_{\text{H}_2}\varepsilon_{\text{CH}_3\text{OH}}}}{k_{\text{Boltzmann}}} \approx 123\text{K} \qquad (70)$$

Equation 70 is essentially an empirical *mixture rule* that allows one to estimate force constants between dissimilar molecules via force constants for pure gases (19). Hence, the Lennard–Jones characteristic temperature for mixtures of C≡O, H_2 and CH_3OH is approximately 123K in equation 67 for the diffusion collision integral. Following the numerical procedures described in the previous section, integration of equation 69 from the external catalytic surface to the central core yields predictions of maximum dimensionless temperature that depend on the Prater number, as illustrated in Figure 5. It is assumed that the temperature polynomials (29) for pure-component specific heats $C_{p,i}(T)$ are valid at reasonably high temperatures near the center of the pellet.

2.16. Consideration of Thermal Diffusion in Pseudo-Binary Mixtures. The preceding analysis of coupled heat and mass transfer in macroporous catalysts with exothermic chemical reaction in the diffusion-controlled regime suggests that predictions of maximum intrapellet temperatures could be significantly larger than those calculated from the Prater equation (ie, $\Theta_{\max} \approx 1 + \beta$) when the Prater number, defined by equation 64, is greater than 0.30. Furthermore, steady-state analysis of the methanol synthesis from carbon monoxide and hydrogen is not a reasonable assumption when the Prater number approaches unity because maximum intrapellet temperatures could be more than an order of magnitude greater than T_{Surface}. The extreme upper limit of the Prater number for realistic steady-state intrapellet simulations decreases from 2.0 to 1.25–1.35 to < 1.0, respectively, as the temperature dependencies of ordinary molecular diffusion coefficients for hard spheres (ie, $T^{3/2}$), the collision integral $\Omega_D(T)$, and the enthalpy change for chemical reaction $\Delta H^0{}_{\text{Reaction}}(T)$ are systematically included in the analysis. Further modifications in the prediction of maximum intrapellet temperature for exothermic reactions in macroporous catalysts include contributions from thermal diffusion (2,13,19) to the

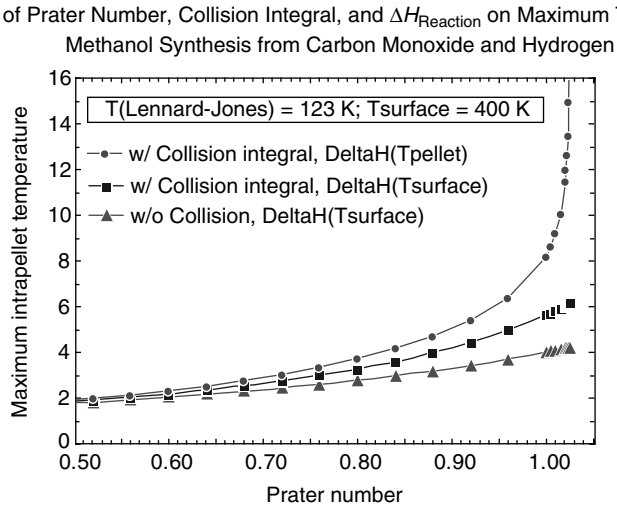

Fig. 5. Effect of the Prater number, the collision integral for ordinary molecular diffusion, and temperature dependence of $\Delta H_{\text{Reaction}}$ on the maximum intrapellet temperature of macroporous catalysts in the diffusion-controlled regime. Calculations are presented for; $CO + 2H_2 \Leftrightarrow CH_3OH$. The Lennard–Jones temperature (or potential well depth, divided by Boltzmann's constant) of 123K represents a geometric average of $\varepsilon_i/k_{\text{Boltzmann}}$ for all three components in the gas mixture (see equation 70). Simulations are presented when temperature on the external catalytic surface is 400K. Inclusion of the collision integral and temperature dependence of in the analysis of coupled heat and mass transfer reveals that steady-state simulations in macroporous catalysts might not be possible when the Prater number approaches unity for the synthesis of methanol.

diffusional mass flux vector (ie, eq. 61) when steep temperature gradients exist within the catalyst.

$$\frac{1}{MW_A} j_{A,\text{pellet}} \approx -D_{A,\text{effective}} \left\{ \nabla C_{A,\text{pellet}} + \frac{\rho}{MW_A} [k_T]_A \nabla \ln T_{\text{pellet}} \right\} \tag{71}$$

Thermal diffusion has been neglected entirely in the classic treatise of diffusion and reaction in permeable catalysts by Aris (1). In equation 71, $[k_T]_A$ is the thermal diffusion ratio for species A, which characterizes the relative importance of thermal diffusion with respect to ordinary molecular diffusion. Both mechanisms in the flux expression of equation 71 are scaled down by intrapellet porosity and tortuosity factors for anisotropic porous catalysts, as illustrated in equation 66 for concentration diffusion. This is a reasonable extension of the parallel-pore model in the presence of thermal diffusion. In binary mixtures of rigid spheres, where the molar masses of both components are very similar, the thermal diffusion ratio for species A is given by (19)

$$\{[k_T]_A\}_{\text{Rigid Sphere}} = \frac{105}{118} \left\{ \frac{MW_A - MW_B}{MW_A + MW_B} \right\} y_A y_B \tag{72}$$

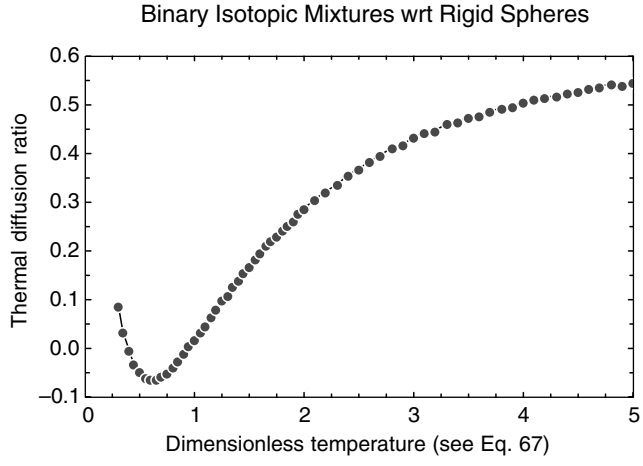

Fig. 6. Universal temperature dependence of the dimensionless thermal diffusion ratio for Lennard–Jones gases, relative to the corresponding ratio for rigid spheres (eq. 72), in binary isotopic mixtures. The dimensionless function $\varphi(T^*)$, defined by equation 73, is plotted vs. dimensionless temperature for Lennard–Jones molecules (eq. 67) as required for the appropriate collision integrals. These data were obtained from pp. 528, 543, 1126–1129, and 1131 in *Molecular Theory of Gases & Liquids* (19).

where y_i is the mole fraction of component i. The thermal diffusion ratio $\varphi_A(T^*)$ for Lennard–Jones molecules, relative to the corresponding ratio for rigid spheres, given by equation 72, is defined as

$$\varphi_A(T^*) = \frac{\left\{[k_T(T^*)]_A\right\}_{\text{Lennard–Jones}}}{\left\{[k_T]_A\right\}_{\text{Rigid Sphere}}} \tag{73}$$

Figure 6 illustrates the universality of $\varphi_A(T^*)$ vs. $T^* = T/T_{\text{Lennard–Jones}}$ for binary isotopic mixtures whose intermolecular forces can be described by the Lennard–Jones 6–12 potential. Inversion temperatures exist when $\varphi_A(T^*) = 0$ for $T^* \approx 0.40$ and $T^* \approx 0.95$. As temperature increases through these inversion points, the direction in which species A diffuses in response to temperature gradients changes. For example, if molecule A is the larger species in binary isotopic mixtures (ie, $MW_A > MW_B$), then its rigid-sphere thermal diffusion ratio is greater than zero, via equation 72, and A diffuses toward lower temperature when $T^* < 0.40$ and $T^* > 0.95$. If $MW_A < MW_B$, then the rigid-sphere thermal diffusion ratio for species A is negative and molecules of type A diffuse toward lower temperature when T^* is between 0.40 and 0.95. This is a crude approximation to the rigorous thermal diffusion ratio of carbon monoxide in ternary gas mixtures with hydrogen and methanol. Equation (8.2–50) in *Molecular Theory of Gases and Liquids* (19) for binary mixtures is expanded in powers of $(MW_A - MW_B)/(MW_A + MW_B)$ and truncated after the linear term when the molar masses of both components are similar.

The universal model illustrated in Figure 6 for Lennard–Jones molecules is valid (30) when $(MW_A - MW_B)/(MW_A + MW_B) < 0.15$. The analog of equation 62 in

the presence of thermal diffusion is a considerably modified Prater equation that, upon numerical integration, yields more sophisticated predictions of maximum intrapellet temperatures relative to the results presented in Figures 4 and 5. Stoichiometry among intrapellet diffusional fluxes, as described by equation 4 for only one chemical reaction, remains valid when thermal diffusion is operative. Hence, the appropriate dimensional equation that describes intrapellet temperature changes is obtained by substituting equation 71 into equation 60. Upon rearrangement, one obtains

$$\frac{\partial T_{\text{pellet}}}{\partial C_{A,\text{pellet}}} = \frac{-D_{A,\text{effective}}(T_{\text{pellet}})\{-\Delta H_{\text{Reaction}}(T_{\text{pellet}})\}}{k_{\text{effective}}\left\{1+\frac{\rho}{MW_A T_{\text{pellet}}} D_{A,\text{effective}}(T_{\text{pellet}})\{-\Delta H_{\text{Reaction}}(T_{\text{pellet}})\}\frac{[k_T(T^*)]_A}{k_{\text{effective}}}\right\}} \tag{74}$$

Dimensional analysis of equation 74 proceeds via the same methodology illustrated in equation 64. Hence, with assistance from the universal temperature-dependent thermal diffusion ratio $\varphi_A(T^*)$ for binary isotopic mixtures, illustrated in Figure 6, one predicts maximum intrapellet temperatures via numerical integration of equation 75 from the external catalytic surface to the central core

$$\frac{\partial \Theta}{\partial \Psi_{A,\text{pellet}}} = \frac{-\beta\varepsilon(\Theta)\zeta(\Theta)}{1+\left\{\frac{\rho}{MW_A C_{A,\text{Surface}}}\right\}\frac{1}{\Theta}\beta\varepsilon(\Theta)\zeta(\Theta)\varphi_A(T^*)\{[k_T]_A\}_{\text{Rigid Sphere}}} \tag{75}$$

Simulations are presented in Figure 7, for $MW_A < MW_B$, and Figure 8, for a wide range of MW_B, to investigate the effect of *thermal diffusion inversion* in pseudo-binary isotopic mixtures on the maximum temperature within macroporous catalysts in the diffusion-controlled regime. When carbon monoxide is the smaller of the two components in pseudo-binary isotopic mixtures, C≡O migrates toward higher temperature regions in the central core of porous catalysts with exothermic chemical reaction for dimensionless temperatures $T^* > 0.95$ (ie, see eqs. 67 and 72; and Figure 6). These conditions are simulated in Figure 7, revealing that the enhanced molar flux of C≡O toward the central core via thermal diffusion, together with temperature dependence for all physicochemical parameters in equation 75, yields the largest prediction of maximum intrapellet temperatures. Relative to simulations that only account for temperature dependence of effective intrapellet diffusivities and $\Delta H_{\text{Reaction}}$, consideration of thermal diffusion (ie, $MW_A < MW_B$) on maximum intrapellet temperatures in Figure 7 is insignificant unless the Prater number is very close to unity.

In contrast, when C≡O is the larger of the two components in pseudo-binary mixtures, it migrates toward lower temperatures near the external catalytic surface for $T^* > 0.95$, impeding the *net diffusional flux* of C≡O toward the central core. Simulations in Figure 8 for exothermic chemical reaction and Prater numbers greater than 0.75 indicate that maximum intrapellet temperatures in the presence of thermal diffusion with $MW_A > MW_B$ are *less* than those predicted by equation 69 when thermal diffusion is neglected (ie, $MW_A = MW_B = 28$ daltons in Figure 8), but all other physicochemical parameters exhibit temperature dependence.

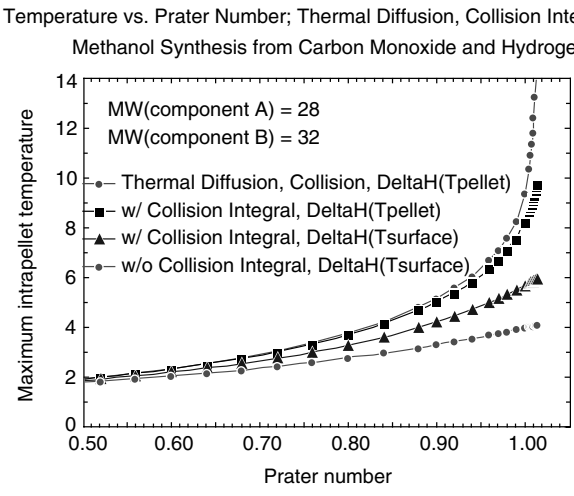

Fig. 7. Effect of the Prater number, thermal diffusion, the collision integral for ordinary molecular diffusion, and temperature dependence of $\Delta H_{\text{Reaction}}$ on the maximum dimensionless intrapellet temperature within macroporous catalysts in the diffusion-controlled regime. Calculations are presented for; $CO + 2\,H_2 \Leftrightarrow CH_3OH$. The Lennard–Jones temperature (or potential well depth, divided by Boltzmann's constant) of 123K represents a geometric average of $\varepsilon_i/k_{\text{Boltzmann}}$ for all three components in the gas mixture (see eq. 70). Simulations are presented when temperature on the external catalytic surface is 400K, and the molecular weight of component A (i.e., $MW_{CO} = 28$ daltons) is less than that of "component B" (i.e., $MW_B = 32$ daltons) in pseudo-binary mixtures.

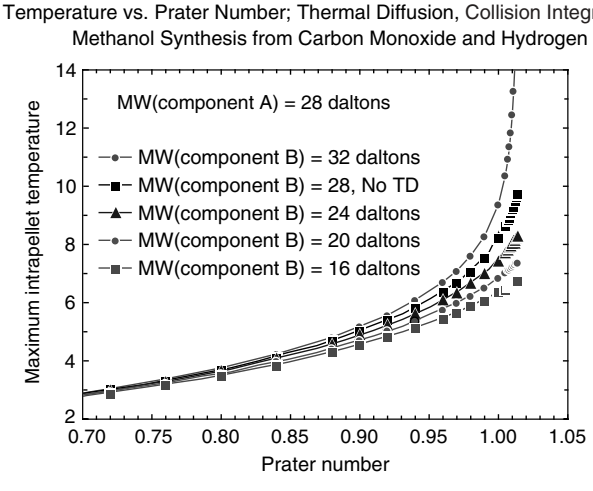

Fig. 8. Effect of the Prater number, thermal diffusion, the collision integral for ordinary molecular diffusion, and temperature dependence of $\Delta H_{\text{Reaction}}$ on the maximum dimensionless intrapellet temperature within macroporous catalysts in the diffusion-controlled regime. Calculations are presented for; $CO + 2\,H_2 \Leftrightarrow CH_3OH$. The Lennard–Jones temperature (or potential well depth, divided by Boltzmann's constant) of 123K represents a geometric average of $\varepsilon_i/k_{\text{Boltzmann}}$ for all three components in the gas mixture (see eq. 70). Simulations are presented when temperature on the external catalytic surface is 400K, and the molecular weight of component A (ie, C≡O) is 28 daltons. The effect of the molecular weight of "component B" in pseudo-binary mixtures is indicated in the legend. Thermal diffusion does not affect these simulations when the molecular weights of both components are the same (see eq. 72).

3. The Complete Strategy for Ideal Nonisothermal Packed Catalytic Tubular Reactors

When porous pellets are packed in tubular reactors and the external resistances to both heat and mass transfer cannot be neglected, it is necessary to predict temperature T_{Surface} and reactant molar density $C_{A,\text{Surface}}$ on the external catalytic surface. The appropriate initial guesses are based on bulk conditions at the reactor inlet. With assistance from effectiveness factor correlations, the rate of reactant consumption is averaged volumetrically throughout the catalyst by evaluating heterogeneous rate laws using conditions on the external catalytic surface. Hence, the appropriate sequence of calculations is (*1*) predict $C_{A,\text{Surface}}$ and T_{Surface} via coupled heat and mass transfer principles discussed earlier in this article (ie, eqs. 8, 18, 22, and 58), (*2*) calculate the intrapellet Damköhler number for reactant A on the external catalytic surface, (*3*) estimate the effectiveness factor via dimensionless correlations that consider catalyst geometry and the kinetic rate law, (*4*) predict a volumetric average of the rate of reactant consumption throughout the catalyst, and (*5*) solve coupled plug-flow differential mass and thermal energy balances to estimate changes in temperature and reactant molar density within the bulk gas phase. The mathematical description of this strategy is summarized below:

(1) Use bulk conditions at the reactor inlet, $C_{A,\text{BulkGas}}(z=0)$ and $T_{\text{BulkGas}}(z=0)$, to estimate the intrapellet Damköhler number $\Lambda^2{}_{A,\text{intrapellet}}$ and the corresponding effectiveness factor E via dimensionless correlations that account for catalyst geometry and the appropriate kinetic rate law (ie, nth-order kinetics). The characteristic length L in the definition of the intrapellet Damköhler number is the radius of spherical catalytic pellets for the analytical correlation given by equation 58 for first-order irreversible chemical kinetics. If the kinetics are not zeroth- or first-order, then numerical methods are required to calculate the effectiveness factor (2).

(2) As $C_{i,\text{BulkGas}}$ at the reactor inlet is known via the nature of the feed stream, one should obtain an iterative solution to the following set of coupled nonlinear algebraic equations to predict $C_{A,\text{Surface}}$, $C_{i,\text{Surface}}$, and T_{Surface} *near* the reactor inlet:

$$k_{A,\text{MTC}}(C_{A,\text{BulkGas}} - C_{A,\text{Surface}})S_{\text{external}} = ES_m\rho_{\text{apparent}}k_{n,\text{Surface}}C^n_{A,\text{Surface}}V_{\text{catalyst}}$$

$$\frac{1}{\upsilon_i}k_{i,\text{MTC}}(C_{i,\text{Surface}} - C_{i,\text{BulkGas}}) = k_{A,\text{MTC}}(C_{A,\text{BulkGas}} - C_{A,\text{Surface}})$$

$$h_{\text{HTC}}\{T_{\text{Surface}} - T_{\text{BulkGas}}\} = (-\Delta H_{\text{Reaction}})k_{A,\text{MTC}}\{C_{A,\text{BulkGas}} - C_{A,\text{Surface}}\}$$

$$\Lambda^2_{A,\text{intrapellet}} = \frac{S_m\rho_{\text{apparent}}k_{n,\text{Surface}}(T_{\text{Surface}})R^2_{\text{sphere}}C^{n-1}_{A,\text{Surface}}}{D_{A,\text{effective}}(T_{\text{Surface}})}$$

$$E = f(\Lambda^2_{A,\text{intrapellet}}; n, \text{CatalystGeometry}) \tag{76}$$

All of these expressions have been discussed earlier in this article. For example, see equations 8, 18, 22, and 58. Each iteration requires a recalculation of the intrapellet Damköhler number and the effectiveness factor (ie, analytical or numerical) at the prevailing values of $C_{A,\text{Surface}}$ and T_{Surface}. Gas-phase mass transfer coefficients for species A (ie, $k_{A,\text{MTC}}$) and species i (ie, $k_{i,\text{MTC}}$) in the first three equations of 76 should be evaluated via equation (22.3-43) or (22.3-44) in *Transport Phenomena*, by Bird et al. (13). For creeping flow around solid spheres, the Sherwood number for mass transfer scales as the one-third power of the particle-based mass transfer Peclet number (2,13) (ie, Pe_{particle}), which incorporates the equivalent diameter of a single catalytic pellet, the average interstitial fluid velocity through the packed bed, and ordinary molecular diffusion coefficients that are evaluated at an average temperature between the bulk gas phase and the external catalytic surface. The corresponding heat transfer coefficient (ie, h_{HTC}) in the third equation of 76 should be evaluated using equation (14.5–2) or (14.5–6) in *Transport Phenomena* (13). All of these heat and mass transfer correlations are consistent with two-dimensional creeping flow of incompressible fluids adjacent to high-shear, no-slip interfaces.

(3) When convergence is obtained to equations 76 for $C_{A,\text{Surface}}$, $C_{i,\text{Surface}}$, and T_{Surface} near the reactor inlet, it is possible to (*1*) use the current value of the effectiveness factor, (*2*) predict the volumetric rate of consumption of reactant A throughout the pellets via effectiveness factor formalism, and (*3*) employ numerical methods like the Runge–Kutta–Gill fourth-order-correct integration algorithm to solve coupled *dimensional* mass and thermal energy balances for ideal gas-phase plug-flow tubular reactors that include the effectiveness factor in the kinetic rate law. The first term on the right side of the one-dimensional thermal energy balance (ie, second equation in 77), which reduces the bulk gas temperature, represents heat transfer to the surroundings because the reactor is not insulated. The second term on the right side of the thermal energy balance represents heat generation due to exothermic chemical reaction. The primary objective is to predict $C_{A,\text{BulkGas}}$, $C_{i,\text{BulkGas}}$, and T_{BulkGas} at a small distance z downstream from their values at the reactor inlet.

$$
\begin{aligned}
q\frac{dC_{A,\text{BulkGas}}}{dV_{\text{Reactor}}} &= -(1-\varepsilon_{p,\text{interpellet}})ES_m\rho_{\text{apparent}}k_{n,\text{Surface}}C^n_{A,\text{Surface}} \\
q\rho_{\text{BulkGas}}C_{p,\text{mixture}}\frac{dT_{\text{BulkGas}}}{dV_{\text{Reactor}}} &= -\left\{\frac{dQ_{\text{output}}}{dV_{\text{Reactor}}}\right\}_{@\text{wall}} \\
&\quad + (-\Delta H_{\text{Rx}})(1-\varepsilon_{p,\text{interpellet}})ES_m\rho_{\text{apparent}}k_{n,\text{Surface}}C^n_{A,\text{Surface}} \\
C_{i,\text{BulkGas}} &= C_{i,\text{BulkGas,Inlet}} + \upsilon_i\{C_{A,\text{BulkGas,Inlet}} - C_{A,\text{BulkGas}}\}
\end{aligned}
\qquad (77)
$$

(4) Use values for $C_{A,\text{Surface}}$, $C_{i,\text{Surface}}$, and T_{Surface} that were obtained from convergence of equations 76 in *step 2*, which includes the most up-to-date values of the intrapellet Damköhler number and the effectiveness factor; update bulk gas molar densities and temperature from the solution

of equations 77 in *step 3*; and obtain another iterative solution to equations 76 in *step 2*. The primary objective is to predict $C_{A,\text{Surface}}$, $C_{i,\text{Surface}}$, and T_{Surface} slightly downstream from their previous values.

(5) Repeat *step 3* and *step 4* to predict molar densities and temperatures in the bulk gas phase and on the external surface of the catalyst from inlet to outlet of the packed catalytic tubular reactor.

There is some discrepancy in the chemical engineering textbook literature about the use of superficial (ie, $\langle v_z \rangle_{\text{superficial}}$) (2,4,6,15,31) vs. interstitial (ie, $\langle v_z \rangle_{\text{interstitial}}$) (2,5,32) average fluid velocity to describe convective transport in the plug-flow mass and thermal energy balances (ie, eqs. 77) for packed catalytic tubular reactors.

3.1. Numerical Analysis of Pseudo-First-Order Irreversible Chemical Kinetics in Ideal Packed Catalytic Tubular Reactors When the External Resistances to Heat and Mass Transfer Cannot be Neglected. *Production of Methanol from a Moderately High-Pressure Stoichiometric Feed of Carbon Monoxide and Hydrogen.* This realistic example implements the complete strategy outlined in the previous section to simulate ideal reactor performance at high mass and heat transfer Peclet numbers, when reactants are consumed by approximate first-order irreversible kinetics on the internal surface of porous spherical pellets. The catalyst is distributed uniformly in a fixed-bed arrangement. The synthesis of methanol from C≡O and H_2 in gas-phase packed catalytic tubular reactors is industrially important. Consequently, a large amount of experimental data is available to characterize this reaction over a wide range of operating pressures (24–28). For simplicity, the effectiveness factor is calculated analytically via the classic isothermal expression in spherical coordinates, given by equation 58. The cgs system of units is employed in the following analysis.

Design Parameters for Ideal Tubular Reactor Performance When External Resistances to Heat and Mass Transfer are Considered. Most of the parametric values, summarized below, are self-explanatory. The interaction energy that governs molecular trajectories and binary collisions is assumed to follow the Lennard–Jones 6-12 potential function. The collision diameter σ and the depth of the potential well (discussed earlier in this article) are required to calculate collision integrals for viscosity and ordinary molecular diffusion (13), as well as the important dimensionless numbers (ie, Reynolds, Schmidt, Prandtl, and Damköhler) that are necessary to estimate interphase heat and mass transfer coefficients, and the effectiveness factor. An integral formulation of linear least-squares regression for continuous objective functions is employed to quantify *reversible* heterogeneous catalytic reactions using first-order irreversible rate laws [ie, $k_{1,\text{Pseudo-Volumetric}} C_{A,\text{inlet}}(\xi_{\text{equilibrium}} - \xi)$], where $\xi_{\text{equilibrium}}$ is the equilibrium conversion of carbon monoxide (C≡O) that depends on the local external catalytic surface temperature T_{Surface} and pressure at each axial position in the tubular reactor (2). As there are no H–H bonds in the final product, the 5-site chemical reaction between adsorbed species on zinc chromite catalysts (ie, ZnO/Cr_2O_3) (2,24,25) is considered to be the rate-limiting step for $CO + 2H_2 \Leftrightarrow CH_3OH$, with nonpreferential dissociative adsorption of atomic hydrogen (ie, H) on adjacent active sites. The synthesis of methanol over

Cu-based catalysts (26) seems to occur exclusively by CO_2 hydrogenation at lower operating pressures. Under nonideal conditions, kinetic rate laws should be constructed using fugacities instead of molar densities or partial pressure (2,27).

Length of the packed catalytic tubular reactor = 325 cm.

Radius of the packed catalytic tubular reactor = 7 cm.

Radius of each porous catalytic pellet (spherical) = 0.7 cm.

Average catalytic pore radius = 10 nm.

Approximate Lennard–Jones collision diameter σ for CO in ternary gas mixtures $\approx$3.5 Å.

Approximate (ie, geometric average) Lennard–Jones potential well depth (2,19) for ternary gas mixtures of C≡O, H_2, and CH_3OH; $\varepsilon_{ABC}/k_{Boltzmann} \approx \{\varepsilon_{CO}\varepsilon_{H_2}\varepsilon_{CH_3OH}\}^{1/3}/k_{Boltzmann} \approx 123K$, via equation 70.

Tortuosity factor for individual porous catalytic pellets = 2.

Intrapellet porosity or void volume fraction for each catalytic pellet = 0.60.

Interpellet porosity or void volume fraction of the entire packed bed = 0.35.

Volumetric flowrate of bulk gas through the packed bed = 100 cm^3/s (ie, 6 L/min).

Average residence time = 175 s.

Ambient temperature = 298K.

Inlet bulk gas temperature = 498K (nonisothermal) or 528K (isothermal).

Inlet total pressure = 50 atmospheres.

Standard state entropy change for $CO + 2H_2 \Leftrightarrow CH_3OH$; $\Delta S^0_{Rx,298K} \approx -53$ cal/mol-K.

Standard state enthalpy change (exothermic chemical reaction); $\Delta H^0_{Rx,298} \approx -21.7$ kcal/mol.

Arrhenius activation energy (33) for the forward reaction = 22.7 kcal/mol.

Pre-exponential factor for pseudo-first-order Arrhenius kinetic rate constant $\approx 3 \times 10^6\ s^{-1}$.

Overall heat transfer coefficient (to the surroundings) = 6×10^{-4} cal/cm^2-s-K.

Stoichiometric feed (ie, 1:2) of C≡O and H_2 at the reactor inlet.

Axial step size for numerical integration = $\Delta\zeta_{PFR} = 10^{-4}$; $0 \le \zeta_{PFR} = z/L_{PFR} \le 1$.

Comparison of Analytical and Numerical Solutions for Ideal Isothermal Tubular Reactors. Numerical simulations were compared with the analytical solution (ie, eq. 46) when the kinetics are first-order and irreversible, and heat effects due to chemical reaction are negligible. Hence, isothermal operation was simulated at 528K, with external mass transfer resistance included in the analysis, but no temperature gradients anywhere throughout the system. Analytical and numerical solutions for the predicted bulk-gas conversion of carbon monoxide are essentially indistinguishable, but the gas-phase molar density of C≡O near the external catalytic surface is slightly less than its corresponding bulk gas-phase molar density, as expected for reactants.

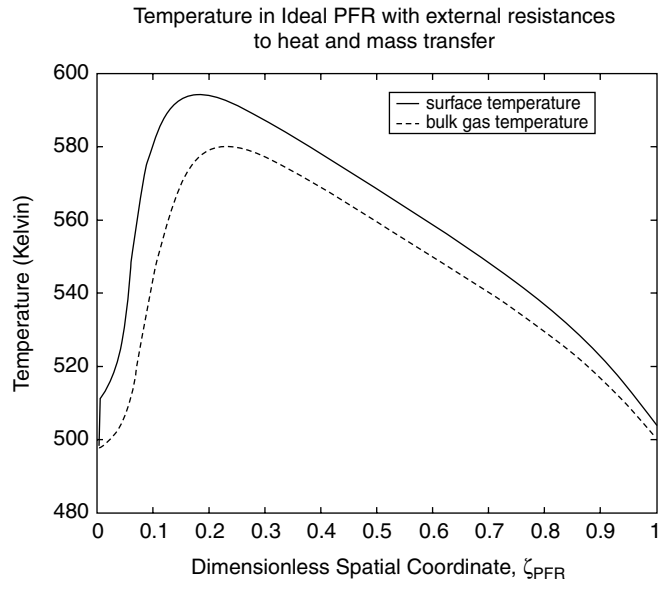

Fig. 9. Temperature profiles in the bulk gas phase (ie, dashed line; T_{BulkGas}) and near the external surface of porous catalytic pellets (ie, solid line; T_{Surface}) for the production of methanol from carbon monoxide and hydrogen in ideal tubular reactors that are not insulated from the surroundings. The $\approx$80K increase in reactor temperature relative to $T_{\mathrm{BulkGas,Inlet}}$, 20% of the reactor length downstream from the inlet, is attributed to exothermic chemical reaction. All simulation parameters are defined in the text. The horizontal coordinate ζ_{PFR} represents dimensionless axial position in the direction of bulk flow, measured from the reactor inlet.

Nonisothermal Tubular Reactor Performance. The influence of external resistances to heat and mass transfer was analyzed in ideal plug-flow reactors without interpellet axial dispersion in the species mass balance or axial conduction in the thermal energy balance. The difference between bulk gas and surface temperatures is proportional to the external heat transfer resistance. Analogously, the difference between species molar density near the external catalytic surface and in the bulk gas phase scales linearly with the external resistance to mass transfer. Using the parameters defined earlier in this section, temperature profiles in the bulk gas stream and near the external surface of the catalytic pellets are illustrated in Figure 9.

The corresponding reactant (ie, C≡O) molar densities are presented in Figure 10. C≡O conversion ξ is defined by *one minus dimensionless molar density in the bulk gas phase* (ie, $\xi = 1 - \Psi_{A,\mathrm{BulkGas}}$). Simulations reveal that the maximum difference between external catalytic surface temperature and bulk gas temperature [ie, $(T_{\mathrm{Surface}} - T_{\mathrm{BulkGas}})_{\max} \approx 40\mathrm{K}$] occurs at approximately 8% of the reactor length downstream from the inlet, whereas this temperature difference (ie, $T_{\mathrm{Surface}} - T_{\mathrm{BulkGas}}$) is less than 10K much further downstream. As expected for exothermic reactions, temperatures within the porous pellets and near the external catalytic surface should be higher than those in the bulk gas stream. The interplay between the rate of thermal energy generation due to

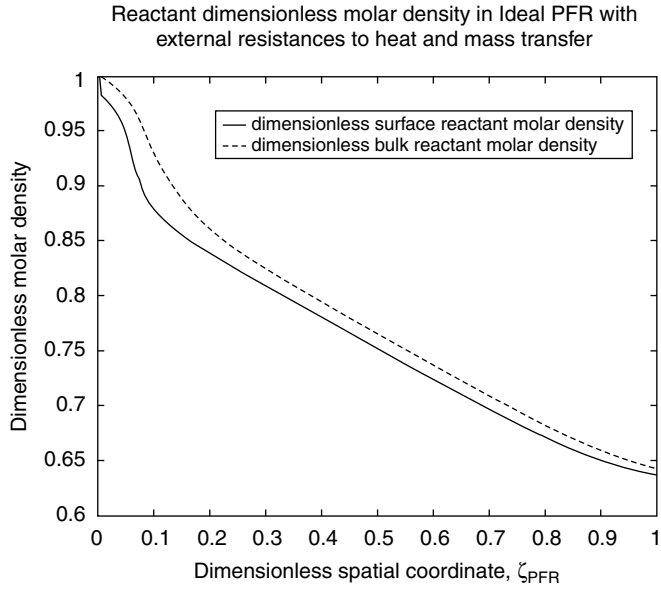

Fig. 10. Dimensionless molar density profiles for carbon monoxide in the bulk gas phase (ie, dashed line; $\Psi_{A,\mathrm{BulkGas}}$) and near the external surface of porous catalytic pellets (ie, solid line; $\Psi_{A,\mathrm{Surface}}$) for the gas-phase production of methanol from a stoichiometric feed of C≡O and H_2 in ideal tubular reactors that are not insulated from the surroundings. Based on simulation parameters defined in the text, the maximum difference between $\Psi_{A,\mathrm{BulkGas}}$ and $\Psi_{A,\mathrm{Surface}}$ occurs at approximately 8% of the reactor length downstream from the inlet [ie, $(\Psi_{A,\mathrm{BulkGas}} - \Psi_{A,\mathrm{Surface}})_{\max} \approx 0.07$ when $\zeta_{\mathrm{PFR}} \approx 0.08$], and ≈35% final conversion of C≡O to CH_3OH is achieved (ie, $\Psi_{A,\mathrm{BulkGas}} \approx 0.65$ when $\zeta_{\mathrm{PFR}} = 1$). The horizontal coordinate ζ_{PFR} represents the dimensionless axial position in the direction of bulk flow, measured from the reactor inlet.

exothermic chemical reaction and the rate of thermal energy removal due to heat transfer across the lateral surface of the reactor governs the maximum temperature increase [$(T_{\mathrm{BulkGas}} - T_{\mathrm{BulkGas,inlet}})_{\max} \approx 80$K in Figure 9], the axial position where maximum temperature occurs, and the overall shapes of the profiles in Figure 9 and Figure 10.

The bulk gas temperature decreases when the rate of heat removal across the lateral surface of the reactor is greater than the generation rate due to exothermic chemical reaction, as described by the second equation in 77. Thermal runaway occurs when the generation rate significantly outweighs the rate of heat removal, producing steep increases in reactor temperature and *near- equilibrium* reactant conversions that might not be described adequately by steady-state analyses. Practical strategies to prevent thermal runaway (2) include (*1*) lowering the inlet temperature of the reactive fluid, (*2*) diluting the feed stream with an inert carrier gas, (*3*) increasing the surface-to-volume ratio of the reactor by decreasing its diameter, and (*4*) increasing the flowrate and lowering the inlet temperature of a cooling fluid that flows either cocurrently or countercurrently with respect to the reactive fluid. One might predict that an increase in bulk gas flowrate of the reactive fluid, which decreases the residence time τ, should

reduce the overall temperature increase, $(T_{\text{BulkGas}} - T_{\text{BulkGas,inlet}})_{\max}$, for exothermic reactions and decrease the final conversion of carbon monoxide. However, decreases in τ and subsequent increases in the mass transfer Peclet number Pe_{MT} reduce external heat and mass transfer resistances in the gas-phase boundary layers surrounding the catalytic pellets. Consequently, the diffusional flux of reactants toward the external catalytic surface increases, reaction rates increase because kinetic rate laws are evaluated at higher reactant molar densities near the external catalytic surface, more thermal energy is generated when reaction rates increase, and the flux of thermal energy from the pellets to the bulk gas phase increases. There is a restricted range of residence times and mass transfer Peclet numbers where all of these sequential effects produce larger increases in reactor temperature and higher conversion, even though shorter residence times suggest that there is less opportunity to convert reactants to products. Isothermally, the effect of residence time, or Pe_{MT}, on reactant conversion is illustrated in Figures 1–3 when the external resistance to mass transfer is important. The study of maximum conversion in nonideal packed catalytic tubular reactors (2), summarized in Table 3, is based on these results. Under nonisothermal conditions, both external resistances are significant near the reactor inlet, and they decrease in magnitude as one approaches the reactor outlet. External transport resistances vanish completely at steady state when there is no chemical reaction. This claim is supported by analyzing all of the coupled nonlinear algebraic equations in *step 2* of the overall strategy (ie, see eqs. 76). In other words, $C_{A,\text{BulkGas}} = C_{A,\text{Surface}}$ and $T_{\text{BulkGas}} = T_{\text{Surface}}$ when $k_{n,\text{Surface}} = 0$. Pellet size, internal pore structure, reactor diameter, and volumetric flowrate represent important design parameters that influence the relative magnitude of external transport resistances, and they should have significant effects on the temperature and molar density profiles illustrated in Figure 9 and Figure 10.

NOMENCLATURE

$C_{A,\text{inlet}}$	molar density of reactant A in the inlet stream to a packed catalytic reactor
$C_{A,\text{pellet}}$	molar density of reactant A within a porous catalytic pellet
C_i	molar density of species i
$C_{i,\text{BulkGas}}$	molar density of species i in the bulk gas phase
$C_{i,\text{BulkGas,Inlet}}$	molar density of species i at the inlet to a packed catalytic tubular reactor
$C_{i,\text{Surface}}$	molar density of gaseous species i near the external surface of a catalytic pellet
$C_{p,i}$	specific heat of pure component i, expressed as a polynomial in T; see equation 69
$C_{p,\text{mixture}}$	mass-fraction-weighted specific heat of the multicomponent gas mixture
$D_{A,\text{effective}}$	effective intrapellet diffusivity of reactant A in porous catalysts

$D_{A,\text{interpellet}}$	interpellet axial dispersion coefficient for reactant A
$D_{A,\text{ordinary}}$	ordinary molecular diffusion coefficient for reactant A
$d_{\text{equivalent}}$	equivalent diameter of irregular-shaped pellets $= 6V_{\text{catalyst}}/S_{\text{external}}$
E	effectiveness factor
$\mathbf{g}_i$	external body force per unit mass acting on species i in a mixture
$\overline{H}_i$	partial molar enthalpy of species i in a mixture
h_{HTC}	heat transfer coefficient in the gas phase boundary layer
$\mathbf{j}_{i,\text{BulkGas}}$	diffusional mass flux of species i in the bulk gas phase
$\mathbf{j}_{i,\text{pellet}}$	diffusional mass flux of species i within a porous catalytic pellet
$k_{\text{Boltzmann}}$	Boltzmann's constant; 1.38066×10^{-23} Joule/K
$k_{1,\text{Pseudo-Volumetric}}$	pseudo-volumetric first-order kinetic rate constant, [=] time^{-1}
$k_{1,\text{Surface}}$	first-order kinetic rate constant for surface-catalyzed chemical reaction (ie, reaction velocity constant), length/time
$k_{n,\text{Surface}}$	nth-order kinetic rate constant for surface-catalyzed chemical reaction, (vol/mol)$^{n-1}$ length/time
$k_{i,\text{MTC}}$	mass transfer coefficient for species i in the gas phase boundary layer
$k_{\text{effective}}$	effective intrapellet thermal conductivity of a porous catalyst
$[k_T]_A$	ratio of the thermal diffusion coefficient to the ordinary molecular diffusion coefficient in equation 71 for the diffusional mass flux of species A
k_{TC}	thermal conductivity of the bulk gas phase surrounding the catalytic pellets
L_{PFR}	length of a packed catalytic tubular reactor
MW_i	molecular weight of species i
m	exponent for the temperature dependence of effective intrapellet diffusion coefficients in macropores (ie, $m = 1.5$) and nanopores (ie, $m = 0.5$)
$\mathbf{n}$	outward directed unit normal vector on surface S that surrounds a chosen volume element V
n	independent spatial variable measured in the direction of $\mathbf{n}$
n (superscript)	reaction order
p	gas phase pressure
Pe_{MT}	vessel-based mass transfer Peclet number that contains $D_{A,\text{interpellet}}$
Pe_{particle}	particle-based mass transfer Peclet number that contains $D_{A,\text{ordinary}}$
q	gas phase volumetric flow rate through the packed catalytic tubular reactor

$\underline{\mathbf{q}}$	molecular flux of thermal energy in multicomponent gas mixtures
Q_{output}	rate of heat transfer to the surroundings across the lateral surface of catalytic tubular reactors
R_k	pseudo-volumetric kinetic rate law for the kth independent chemical reaction
R	pseudo-volumetric kinetic rate law when only one chemical reaction occurs
R_{Surface}	intrinsic kinetic rate law for heterogeneous surface-catalyzed chemical reaction
R_{PFR}	radius of a heterogeneous packed catalytic tubular reactor
R_{sphere}	radius of porous spherical catalytic pellets
Re	Reynolds number based on bulk gas phase properties; the characteristic length corresponds to the length of the packed catalytic tubular reactor
$(\text{Re}Sc)_{\text{critical}}$	critical value of the vessel-based mass transfer Peclet number
S	surface element over which integration occurs via Gauss' law
Sc	Schmidt number based on bulk gas phase properties
S_{external}	external surface area of one porous catalytic pellet
S_m	internal catalytic surface area per unit mass of catalyst
$Sh_{\text{Average,particle}}$	particle-based surface-averaged Sherwood number for mass transfer correlations
t	time
T	temperature in the thermal energy balance
T^*	dimensionless temperature in the diffusion collision integral, equation 67 and on the horizontal axis of Figure 6
T_{BulkGas}	temperature in the bulk gas phase external to the catalytic pellets
$T_{\text{BulkGas,Inlet}}$	temperature of the stoichiometric bulk gas mixture of CO and H_2 at the inlet to the packed catalytic tubular reactor
T_{pellet}	temperature within porous catalytic pellets
T_{Surface}	temperature near the external surface of the catalytic pellets
u	specific internal energy of the gas phase mixture
$\mathbf{v}$	mass-average velocity vector of a multicomponent reactive mixture
$\boldsymbol{v}_{\text{i}}$	velocity vector for species i in a mixture
$\langle v_z \rangle_{\text{interstitial}}$	average interstitial velocity through a packed column (z-component)
$\langle v_z \rangle_{\text{superficial}}$	average superficial velocity through an empty tube (z-component)

V	volume element over which integration occurs
V_{catalyst}	total volume of one porous catalytic pellet
V_{pellet}	total volume of all catalytic pellets in a packed tubular reactor
V_{Reactor}	total volume of a heterogeneous packed catalytic tubular reactor
y_i	mole fraction of component i
z	independent spatial variable in the axial direction for a tubular reactor
Z	axial gradient in the molar density of reactant A

Greek Symbols:

α	parameter defined by equations 45 and 57
β	Prater number, defined in equation 64
γ	exponent in equation 59 for the scaling law between α and $d_{\text{equivalent}}$
∇	gradient operator
$\Delta H_{\text{Reaction}}$	molar enthalpy change for the chemical reaction at temperature T
$\Delta H^0{}_{\text{Rx,298}}$	standard state molar enthalpy change for the chemical reaction at 298K
$\Delta S^0{}_{\text{Rx,298}}$	standard state molar entropy change for the chemical reaction at 298K
$\varepsilon(\Theta)$	ratio of effective intrapellet diffusivities for reactant A, defined in equations 64 and 68
$\varepsilon_{\text{Lennard–Jones}}$	maximum energy of attraction for Lennard–Jones molecules, or maximum depth of the potential well when molecules reside at their equilibrium separation distance
$\varepsilon_{p,\text{interpellet}}$	interpellet porosity of the entire packed catalytic tubular reactor
$\varepsilon_{p,\text{intrapellet}}$	intrapellet porosity, or void volume fraction, of an individual catalytic pellet
$\varphi_{\text{correlation}}$	correlation coefficient for interpellet axial dispersion, defined by equation 55
$\Lambda^2{}_{A,\text{intrapellet}}$	intrapellet Damköhler number of reactant A, defined in equation 76, and required for the effectiveness factor in equation 58
$\Lambda^2{}_{A,\text{interpellet}}$	interpellet Damköhler number of reactant A, based on $D_{A,\text{interpellet}}$ and L_{PFR}, defined by equation 26
υ_{ik}	stoichiometric coefficient of species i in the kth chemical reaction
υ_i	stoichiometric coefficient of species i when there is only one reaction
η	dimensionless intrapellet radial coordinate in porous spherical catalysts; $\eta = \text{r}/\text{R}_{\text{sphere}}$

$\varphi_A\ (T^*)$	thermal diffusion ratio for Lennard–Jones gases relative to that for hard spheres, illustrated as a function of dimensionless temperature T^* in Figure 6 for binary isotopic mixtures
$\rho_{apparent}$	apparent density of a porous catalytic pellet, including occupied and void volume
ρ	total mass density of the gas phase mixture
$\rho_{BulkGas}$	total mass density of the gas phase mixture, external to the catalytic pellets
Θ	dimensionless intrapellet temperature in porous catalysts
Θ_{max}	maximum dimensionless intrapellet temperature near the center of porous catalysts
σ	collision diameter for the Lennard–Jones 6-12 intermolecular potential
τ	residence time, or viscous stress tensor (ie, molecular momentum flux)
$\Psi_{A,BulkGas}$	dimensionless molar density of reactant A in the bulk gas stream
$\Psi_{A,BulkGas,Ideal}$	dimensionless molar density of reactant A in the bulk gas stream for simulations that neglect interpellet axial dispersion
$\Psi_{A,BulkGas,Real}$	dimensionless molar density of reactant A in the bulk gas stream for simulations that include interpellet axial dispersion
$\Psi_{A,pellet}$	dimensionless intrapellet molar density of reactant A in porous catalysts
$\Psi_{A,Surface}$	dimensionless molar density of reactant A near the external surface of a catalytic pellet
$\Psi_{A,Surface,Ideal}$	dimensionless molar density of reactant A near the external surface of a catalytic pellet in simulations that neglect interpellet axial dispersion
$\Psi_{A,Surface,Real}$	dimensionless molar density of reactant A near the external surface of a catalytic pellet in simulations that include interpellet axial dispersion
Ω	dimensionless chemical reaction coefficient; product of interpellet Damköhler number, effectiveness factor, and catalyst filling factor (ie, $1 - \varepsilon_{p,interpellet}$); see equation 29
Ω_D	collision integral for diffusion, parameterized by equation 67
$\zeta(\Theta)$	dimensionless ratio of molar enthalpy changes for chemical reaction, defined by equations 64 and 69
ζ_{PFR}	dimensionless spatial variable in the primary flow direction of a packed catalytic tubular reactor ($= z/L_{PFR}$)
ξ_{PFR}	dimensionless transformed axial coordinate (ie, $1-\zeta_{PFR}$) when numerical integration of the plug-flow mass balance in nonideal reactors is performed backward, from outlet to inlet

ξ	instantaneous conversion of reactant A in a packed catalytic tubular reactor
$\xi_{equilibrium}$	equilibrium conversion of reactant A that depends on $T_{Surface}$ and pressure p
ξ_{final}	final conversion of reactant A in the exit stream of a catalytic reactor
χ	deflection angle for binary molecular collisions in dilute gas mixtures

BIBLIOGRAPHY

"Simultaneous Heat and Mass Transfer" in *ECT* 3rd ed., Vol. 21, pp. 54–76, by L. A. Wenzel, Lehigh University; in *ECT* 4th ed., Vol. 22, pp. 195–222, by L. A. Wenzel, Lehigh University; "Simultaneous Heat and Mass Transfer," in *ECT* (online), posting date: December 4, 2000, by L. A. Wenzel, Lehigh University.

CITED PUBLICATIONS

1. R. Aris, *The Mathematical Theory of Diffusion and Reaction in Permeable Catalysts; Theory of the Steady State*, Vol. 1, Oxford University Press, Bristol, 1975, pp. 53, 96.
2. L. A. Belfiore, *Transport Phenomena for Chemical Reactor Design*, Wiley, Hoboken, NJ, 2003.
3. J. W. Tester and M. Modell, *Thermodynamics and its Applications*, 3rd ed., Prentice-Hall, Upper Saddle River, NJ, 1997, pp. 769–770.
4. H. S. Fogler, *Elements of Chemical Reaction Engineering*, 4th ed., Prentice-Hall, Upper Saddle River, NJ, 2006, p. 958.
5. R. W. Missen, C. A. Mims, and B. A. Saville, *Introduction to Chemical Reaction Engineering and Kinetics*, Wiley, New York, 1999, pp. 525–527.
6. G. F. Froment and K. B. Bischoff, *Chemical Reactor Analysis and Design*, 2nd ed., Wiley, New York, 1990, pp. 184, 497.
7. B. A. Finlayson, *The Method of Weighted Residuals and Variational Principles*, Academic Press, New York, 1972, Chapt. 5.
8. K. B. Bischoff, *Chem. Eng. Sci.* **16**, 131 (1961).
9. P. V. Danckwerts, *Chem. Eng. Sci.* **2**, 1 (1953).
10. I. Langmuir, *J. Am. Chem. Soc.* **30**, 1742 (1908).
11. J. W. Hiby, *Interactions Between Fluids and Solids*, Inst. Chem. Engr., London, 1962, p. 312.
12. E. Wicke, *Chemie Ing. Techn.* **47**, 547 (1975).
13. R. B. Bird, W. E. Stewart, and E. N. Lightfoot, *Transport Phenomena*, 2nd ed., Wiley, Hoboken, NJ, 2002, pp. 441, 686.
14. F. A. L. Dullien, *Porous Media; Fluid Transport and Pore Structure*, 2nd ed., Academic Press, New York, 1992, Chapt. 6.
15. M. E. Davis and R. J. Davis, *Fundamentals of Chemical Reaction Engineering*, McGraw Hill, New York, 2003, pp. 213–218, 317.
16. C. D. Prater, *Chem. Eng. Sci.* **8**, 284 (1958).
17. P. B. Weisz and J. S. Hicks, *Chem. Eng. Sci.* **17**, 265–275 (1962).
18. G. Damköhler, *Z. Phys. Chem.* **A193**, 16 (1943).

19. J. O. Hirschfelder, C. F. Curtiss, and R. B. Bird, *Molecular Theory of Gases and Liquids*, Wiley, New York, 1954.
20. D. A. McQuarrie, *Statistical Mechanics*, University Science Books, Sausalito, CA, 2000, Chapt. 19.
21. P. Resibois and M. de Leener, *Classical Kinetic Theory of Fluids*, Wiley, New York, 1977, pp. 141–142, 372–373.
22. P. D. Neufeld, A. R. Janzen, and R. A. Aziz, *J. Chem. Phys.* **57**, 1100 (1972).
23. J. P. Irving and J. B. Butt, *Chem. Eng. Sci.* **22**, 1859–1873 (1967).
24. K. Klier, V. Chatikavanij, R. G. Herman, and G. W. Simmons, *J. Catalysis* **74**(2), 343–360 (1982).
25. G. Natta, in P. H. Emmett, ed., *Catalysis*, Vol. 3, Reinhold, New York, 1955, pp. 349–411.
26. A. Y. Rozovskii and G. I. Lin, *Top. Catalysis* **22**(3–4), 137–150 (2003).
27. I. K. Gamwo, J. S. Halow, D. Gidaspow, and R. Mostofi, *Chem. Eng. J.* **93**(2), 103–112 (2003).
28. V. E. Leonov, M. M. Karavaev, E. N. Tsybina, and G. S. Petrishcheva, *Kinet. Katal.* **14**, 970–975 (1973).
29. O. A. Hougen, K. M. Watson, and R. A. Ragatz, *Chemical Process Principles, Part 2, Thermodynamics*, Wiley, New York, 1964, Appendix 27–28.
30. E. R. S. Winter, *Trans. Faraday Soc.* **46**, 81 (1950).
31. J. M. Smith, *Chemical Engineering Kinetics*, McGraw-Hill, New York, 1970, p. 502.
32. L. D. Schmidt, *The Engineering of Chemical Reactions*, Oxford University Press, Cary, NC, 1998, pp. 271–272.
33. H. P. Robert and H. C. Cecil, *Chemical Engineers' Handbook*, 5th ed., McGraw-Hill, New York, 1973.

LAURENCE A. BELFIORE
JEREMIAH J. WAY
LI ZHANG
Colorado State University